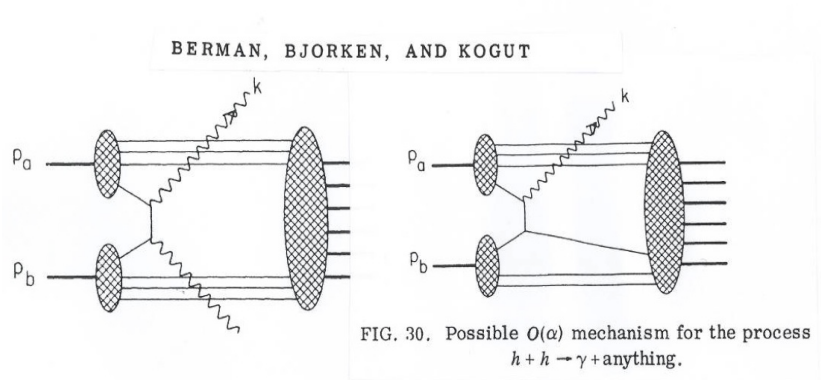
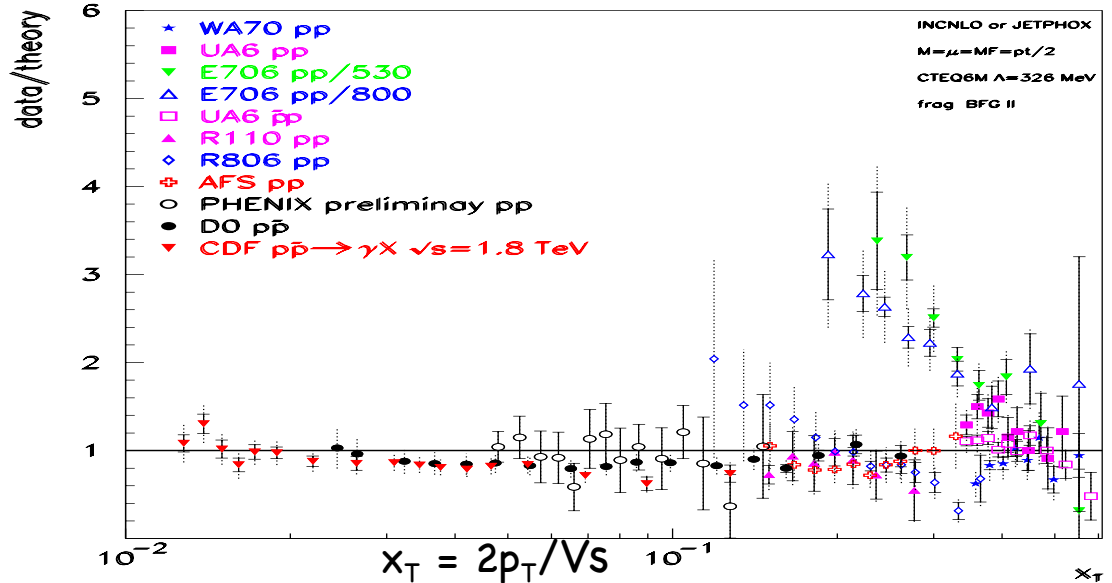


Single and Double Prompt Photons in Hadroproduction

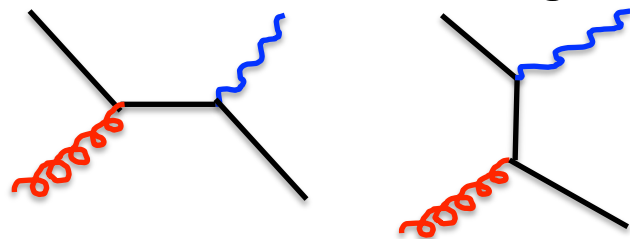
Workshop on Photon Physics
Paris, March 30

NLO
NNLO
Resummation
Isolation
MC, MC + HO



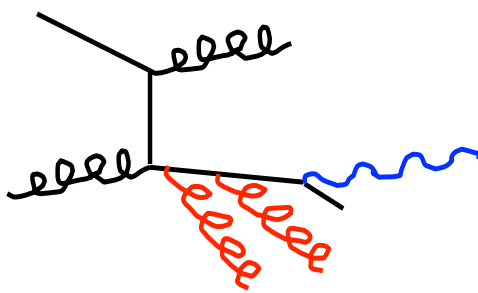
We have little evidence on which hadronic partons exist (indeed, whether the concept is correct). We feel it is relatively futile at this stage to speculate wildly about the nature of strong parton-parton interactions. Therefore, we consider mainly the elementary electromagnetic processes (a)-(e). The results we obtain as mentioned earlier

1977 Fritsch + Minkovski
Tests of QCD
g/P



- Background for New Physics
- Benchmarks for new detectors

NLO



Photon Fragmentation

$$\sigma^B(q + g \rightarrow q + g) \otimes e_q^2 \frac{\alpha}{2\pi} \left\{ \underbrace{\left[-\frac{(4\pi)^\varepsilon}{\varepsilon} \frac{\Gamma(1-\varepsilon)}{\Gamma(1-2\varepsilon)} + \log \frac{M_F^2}{\mu^2} \right] P_{\gamma q}^{(0)}(z) + \underbrace{\left[\log \frac{p_\perp^{\gamma^2}}{M_F^2} + \log(1-z) - \log z \right] P_{\gamma q}^{(0)}(z) + z}_{\text{direct HO}} \right\}$$

$$D_q^\gamma(z, M_F)$$

$$P_{\gamma q} = \frac{\alpha}{2\pi} \left(P_{\gamma q}^{(0)} + \frac{\alpha_s}{2\pi} P_{\gamma q}^{(1)} + \dots \right) C_q$$

$$M^2 \frac{\partial D_q^\gamma}{\partial M^2} = P_{\gamma q} + P_{qq} \otimes D_q^\gamma$$

$$D_{q,NS}^\gamma = D_q^\gamma + D_{\bar{q}}^\gamma - \frac{\sum_q^{\text{NP}} (D_q^\gamma + D_{\bar{q}}^\gamma)}{N_f}$$

$$D(n) = \int_0^1 dz z^{n-1} D(z) \quad D_q^\gamma(M^2, n) = \int \frac{dk^2}{k^2} P_{\gamma q}(n) e^{\int_{k^2}^{M^2} \frac{dp^2}{p^2} P_{qq}(p)} \rightarrow D^{\text{NP}}(M^2, Q_0^2, n) + D^P(M^2, Q_0^2, n)$$

↓

Log(1/1-z)

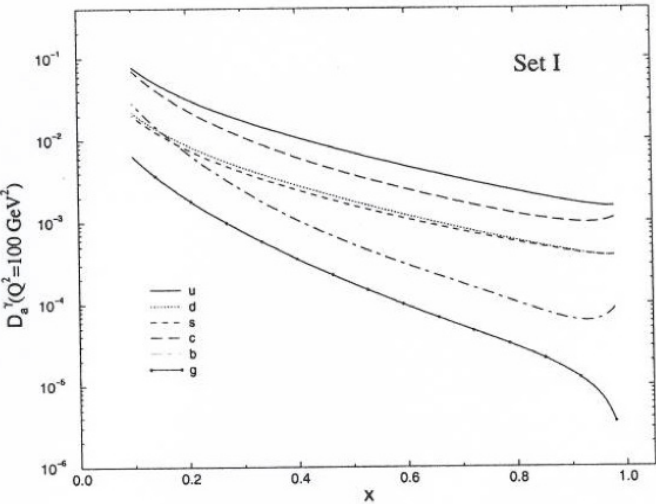


Figure 6: The fragmentation functions at $Q^2 = 100 \text{ GeV}^2$.

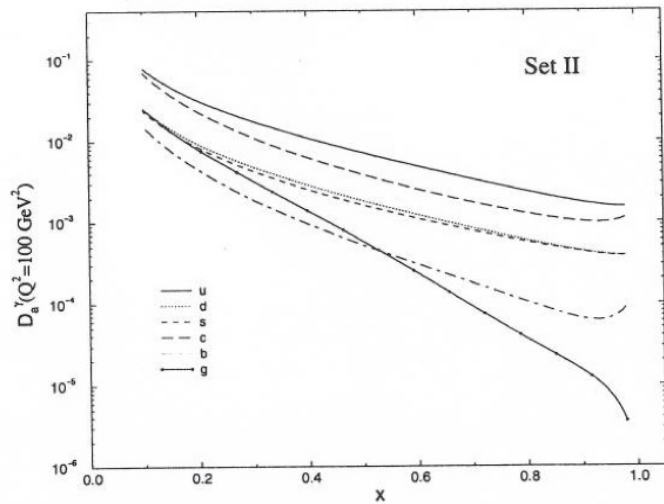


Figure 7: The fragmentation functions at $Q^2 = 100 \text{ GeV}^2$.

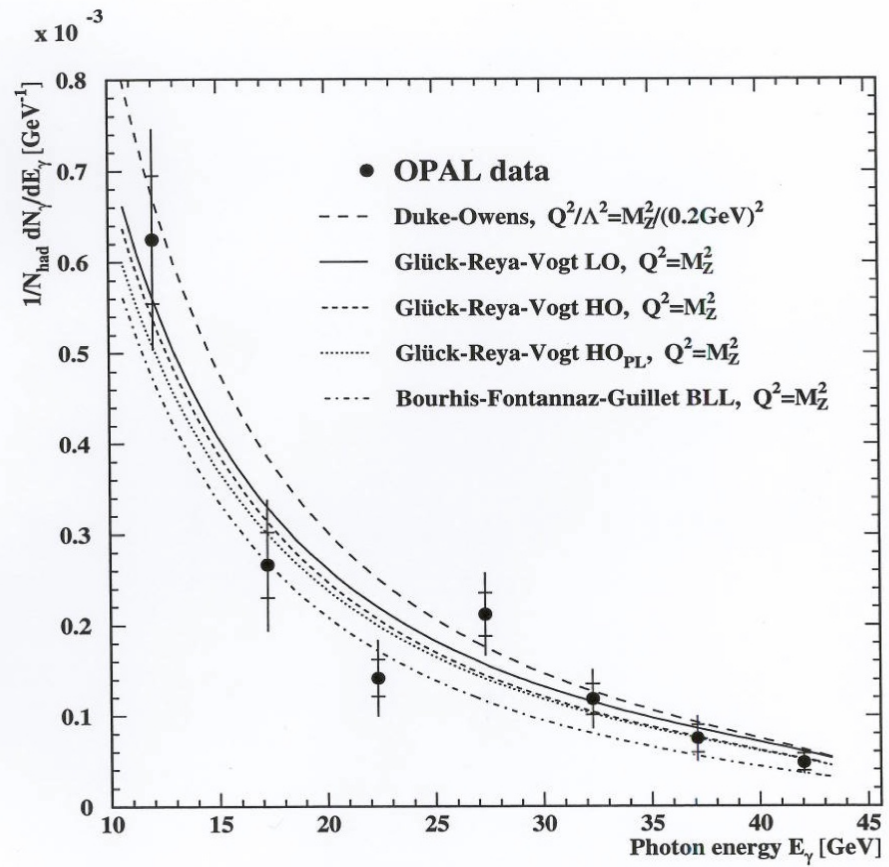


Figure 6: The photon energy spectrum in hadronic Z^0 decays compared to various theoretical predictions: the Duke-Owens parametrisation [8], the Glück, Reya and Vogt predictions including leading-order (LO), higher-order (HO) and higher-order without the non-perturbative corrections (HO_{PL}) [9]. The Bourhis, Fontannaz and Guillet prediction shown include effects beyond leading logarithms (BLL) [10].

GRV: $Q^2_0 = .3 \text{ GeV}^2$

BFG: $Q^2_0 = .5 \text{ GeV}^2$

Constraining the photon fragmentation function

$$Z = - \frac{p_T^\gamma p_T^{\text{jet}} \cos(\phi)}{(p_T^{\text{jet}})^2}$$

RHIC $\sqrt{s} = 200 \text{ GeV}$

$$11 < p_T^{\text{jet}} < 13 \text{ GeV}$$

$$3 < p_T^\gamma < 16 \text{ GeV}$$

$$-.5 < \eta^\gamma < .5$$

$$-1 < \eta^{\text{jet}} < 1$$

Non isolated cross section

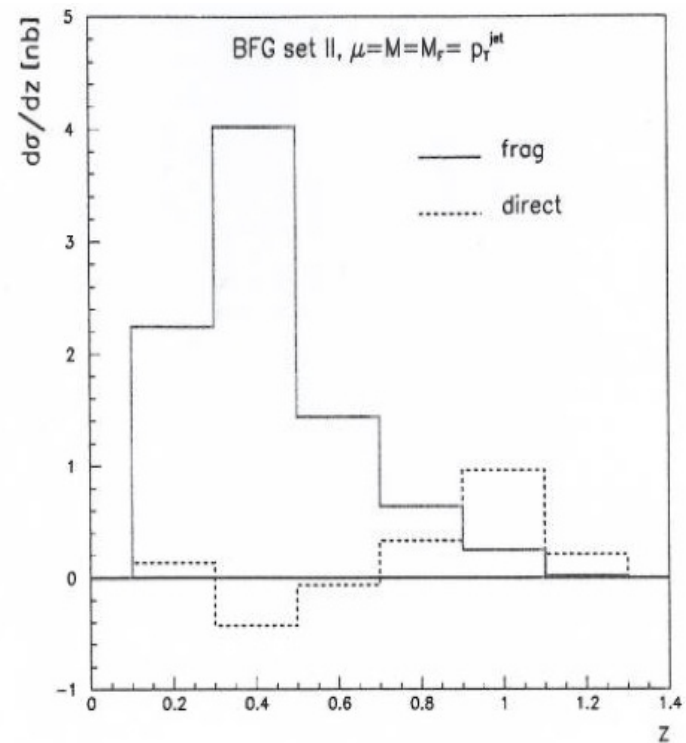


Figure 4: Cross section $d\sigma/dz_\gamma$ for the BFG set II.

Belghobsi
Fontannaz
Guillet
Heinrich
Piløn
Werlen

Isolation

Fixed target ($p_T^\gamma < 10 \text{ GeV}$) π^0 resolved
Colliders isolation

Cone R_c

$$E_T^h < \varepsilon p_T^\gamma \quad z > 1/(1+\varepsilon) = z_c$$

Frixione

$$(p_T^\gamma(1-z)/z) = E_T^h < \varepsilon p_T^\gamma R \quad R < R_c$$

$$\left\{ D(z, M_F) + e_q^2 \frac{\alpha}{2\pi} P_{\gamma q}^{(0)}(z) \left(\log \frac{R_c^2 p_\perp^{\gamma^2}}{M_F^2} + 2 \log(1-z) + \frac{z}{P_{\gamma q}^{(0)}} \right) + O(R_c^2) \right\} \theta(z - z_c) + \log \frac{1}{z(1-z)R_c}$$

$$\int_0^{R_c} \frac{dR^2}{R^2} \theta \left(R - \frac{1}{\varepsilon} \frac{1-z}{z} \right) = 2 \log \frac{z\varepsilon R_c}{1-z} \theta \left(z - \frac{1}{1+\varepsilon R_c} \right)$$

$$R^2 = (y_q - y_\gamma)^2 + (\varphi_q - \varphi_\gamma)^2$$

$$\varepsilon \sim .01 - .1 \quad R_c \sim .4 - 1.$$

JETPHOX

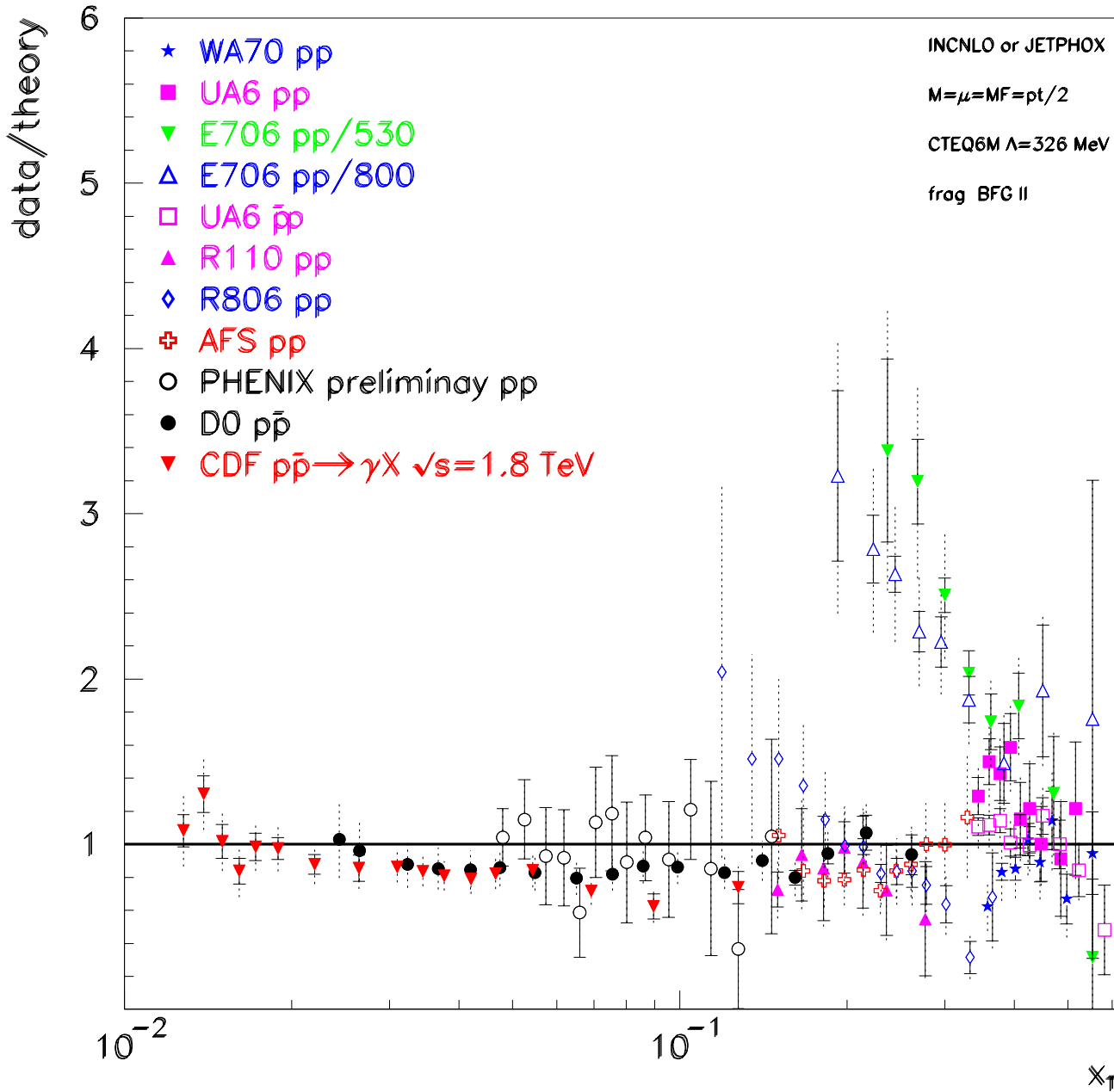
NLO direct

NLO fragmentation

CTEQ6M

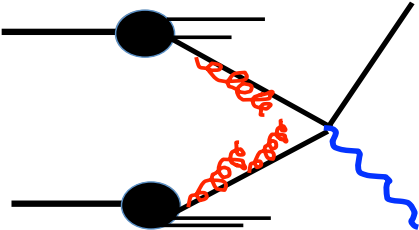
BFG II

$M_I = M_F = \mu = p_T^\gamma$



Aurenche et al.
(2006)

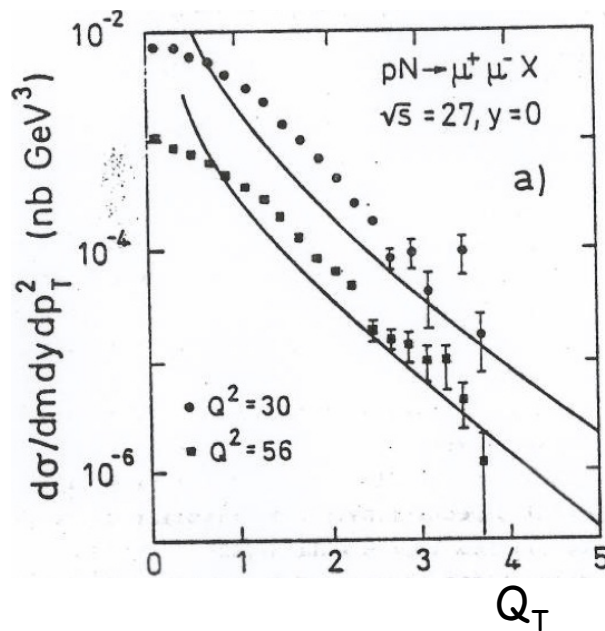
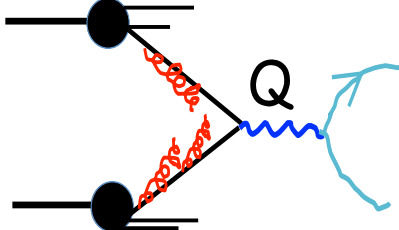
The Primordial k_T of the E706 Experiment



$$\frac{d\sigma}{dp_\perp^\gamma} \sim \int d\vec{k}_{\perp 1} f(\vec{k}_{\perp 1}) \int d\vec{k}_{\perp 2} f(\vec{k}_{\perp 2}) \frac{1}{p_\perp^{\gamma^2} (\vec{p}_\perp^\gamma - \vec{k}_{\perp 1} - \vec{k}_{\perp 2})^2} = \frac{1}{p_\perp^{\gamma^4}} \left(1 + \mathcal{O} \frac{<\kappa_\perp^2>}{p_\perp^{\gamma^2}} \right)$$

$$f = \frac{e^{-\kappa_\perp^2 / <\kappa_\perp^2>}}{\pi <\kappa_\perp^2>} \quad <\kappa_\perp> \simeq 1.3 \text{ GeV/c} \quad (\text{E706})$$

$$<\kappa_\perp> \simeq 3.5 \text{ GeV/c} \quad (\text{CDF})$$

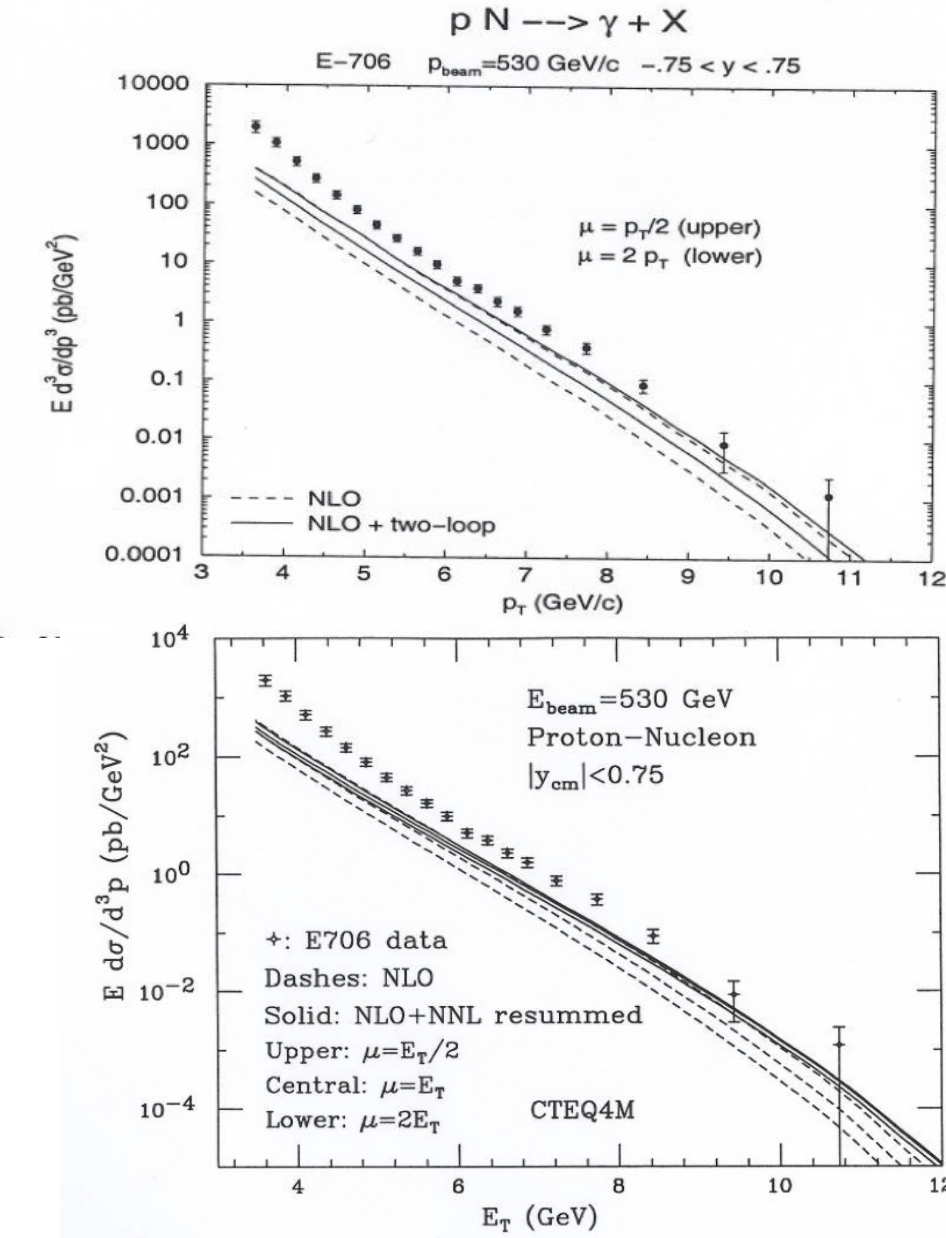
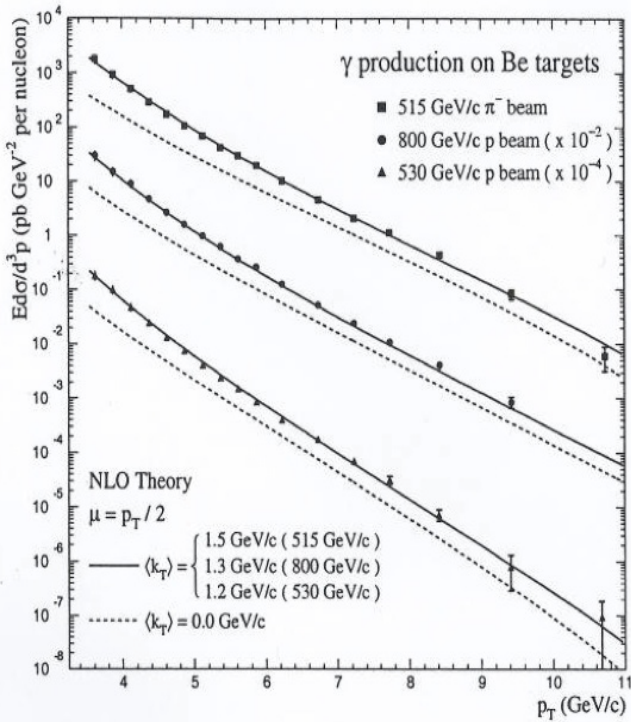


$$\frac{d\hat{\sigma}}{dQ_\perp^2} = \sigma^B(Q^2) \left[\delta(Q_\perp^2) + \frac{\alpha_s}{\pi} \frac{\ln Q^2/Q_\perp^2}{Q_\perp^2} - \delta(Q_\perp^2) \frac{\alpha_s}{\pi} \int_0^{Q^2} \frac{dk_\perp^2}{k_\perp^2} \ln(Q^2/K_\perp^2) \right]$$

$$\int_0^{Q^2} \frac{d\hat{\sigma}}{dQ_\perp^2} dQ_\perp^2 = \sigma^B(Q^2)$$

Kidonakis
Owens

Catani
Mangano
Nason
Oleari
Vogelsang



Theoretical improvements

● k_T -resummation in the $x_T = 2p_T^\gamma / \sqrt{s} \rightarrow 1$ limit $\Rightarrow 25\% \text{ effect}$

(also study of non perturbative contributions)

Laenen
Sterman
Vogelsang

● Threshold resummation: limit $x_T \rightarrow 1$

Improved stability with respect to the scales

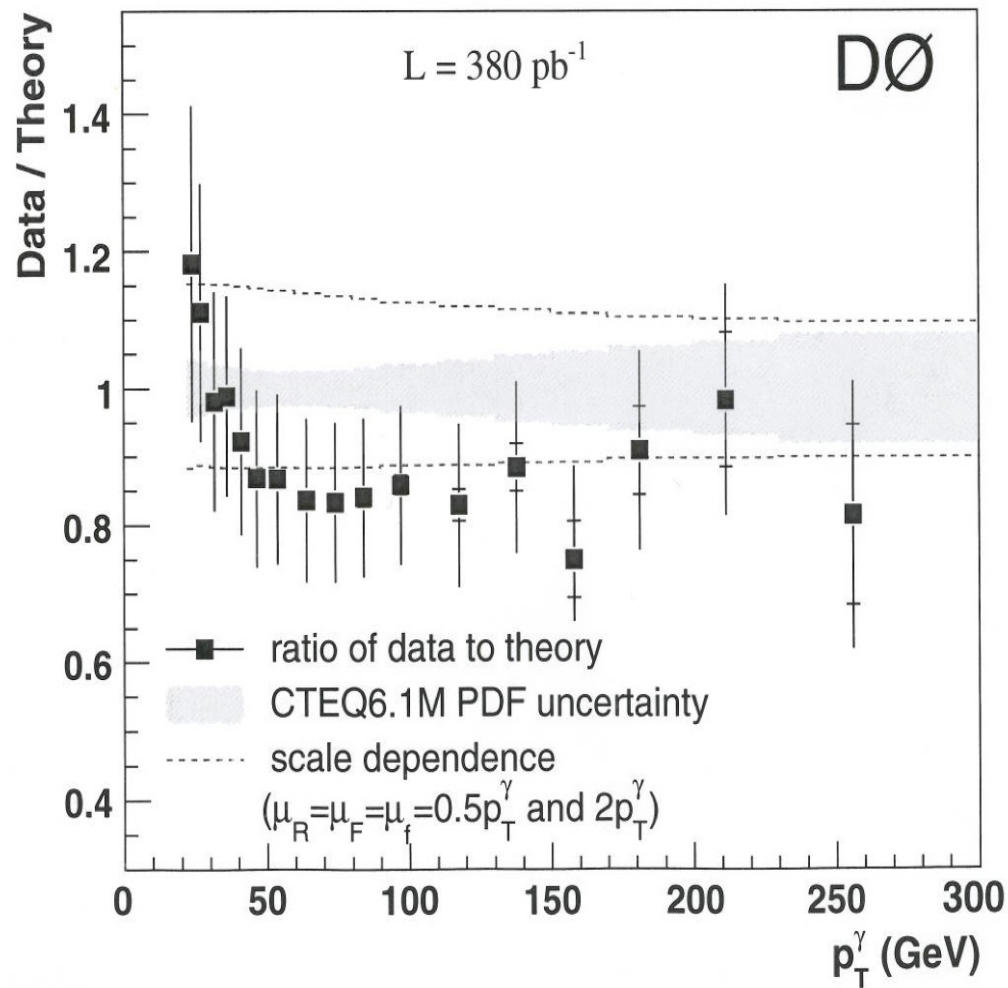
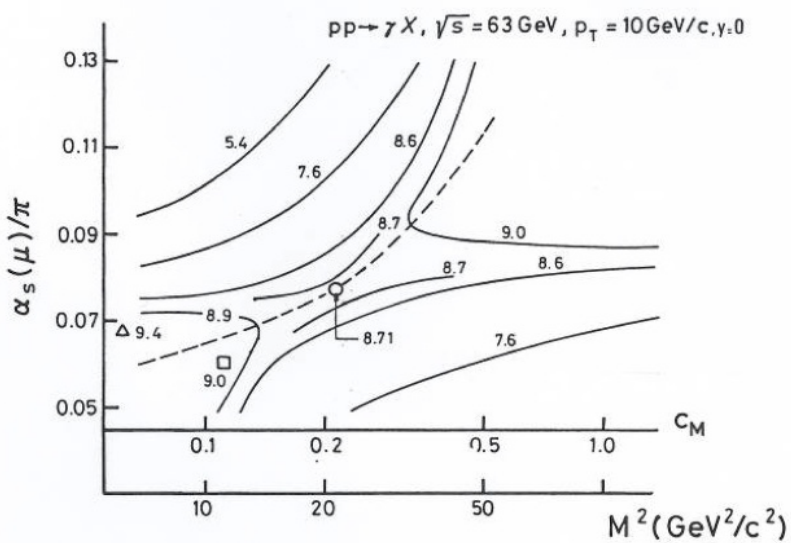
Bonciani,Catani,Mangano,Nason,
Oleari,Vogelsang,
de Florian, Vogelsang

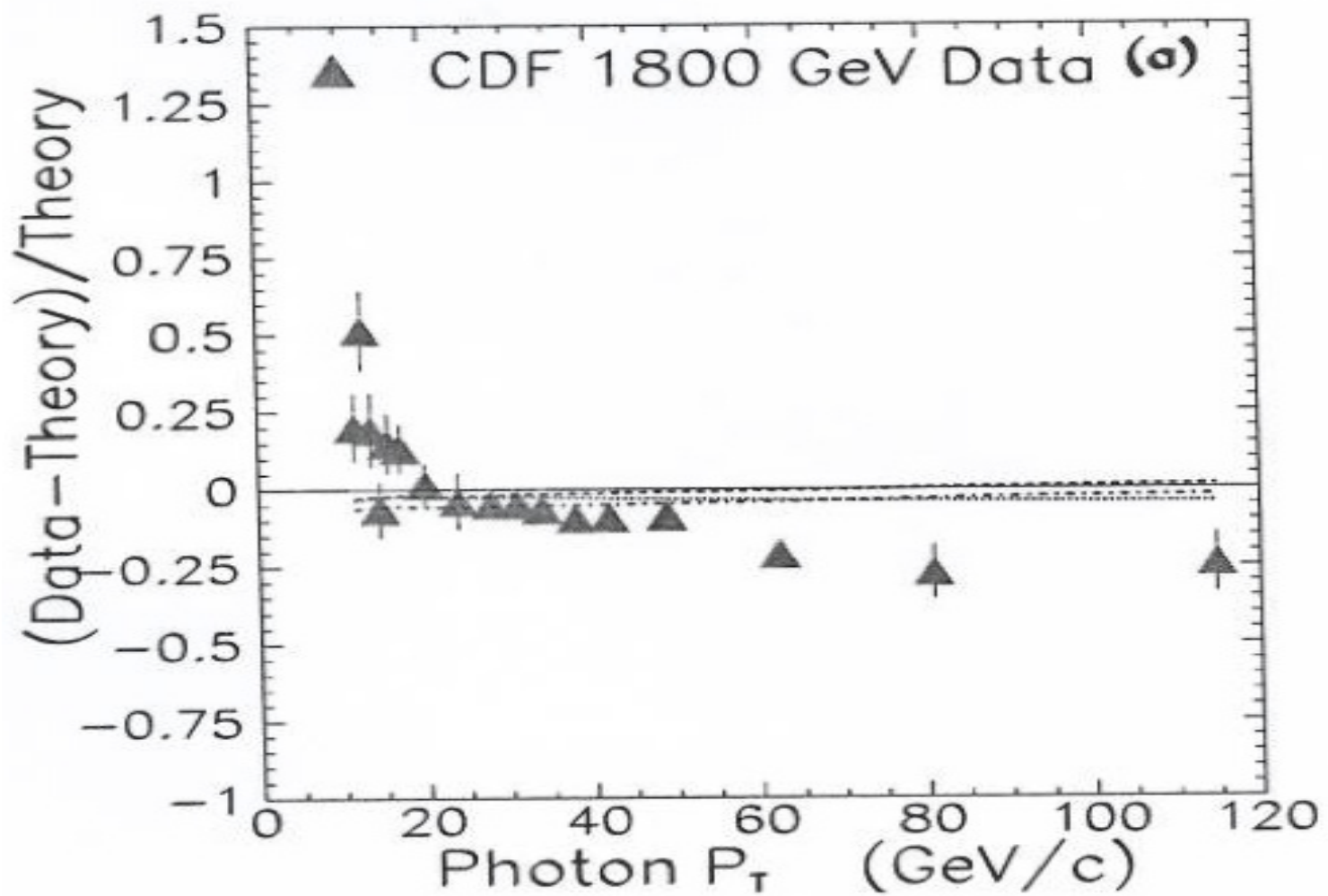
Laenen,Oderda,Sterman
Kidonakis,Owens

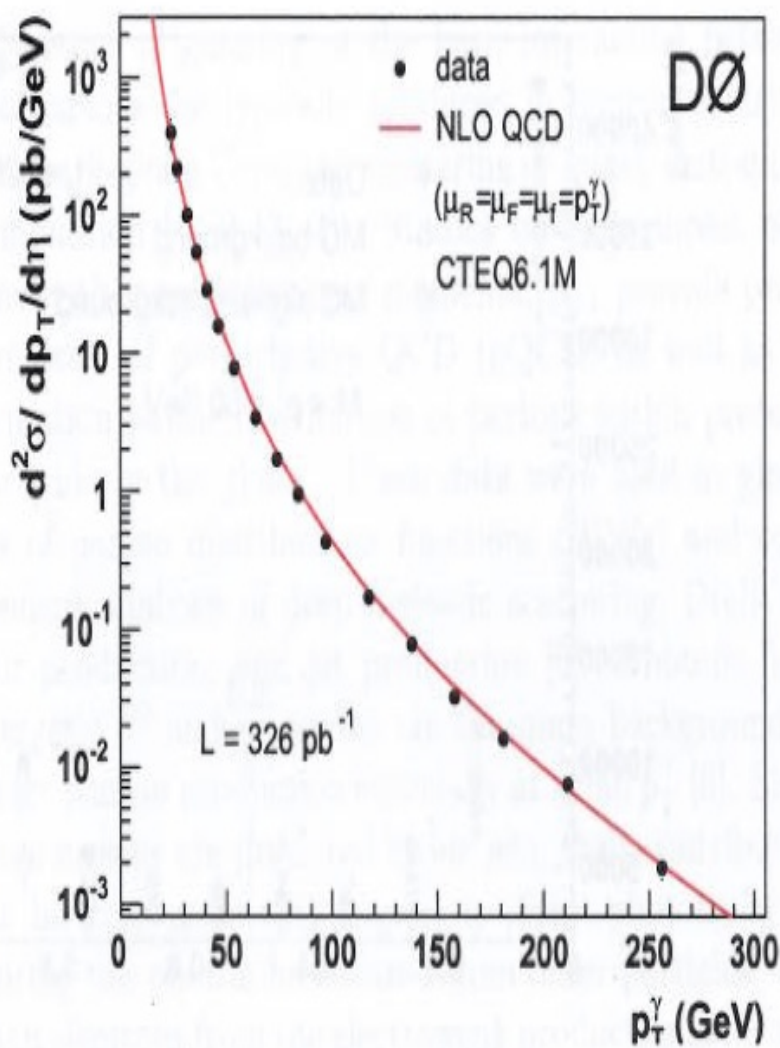
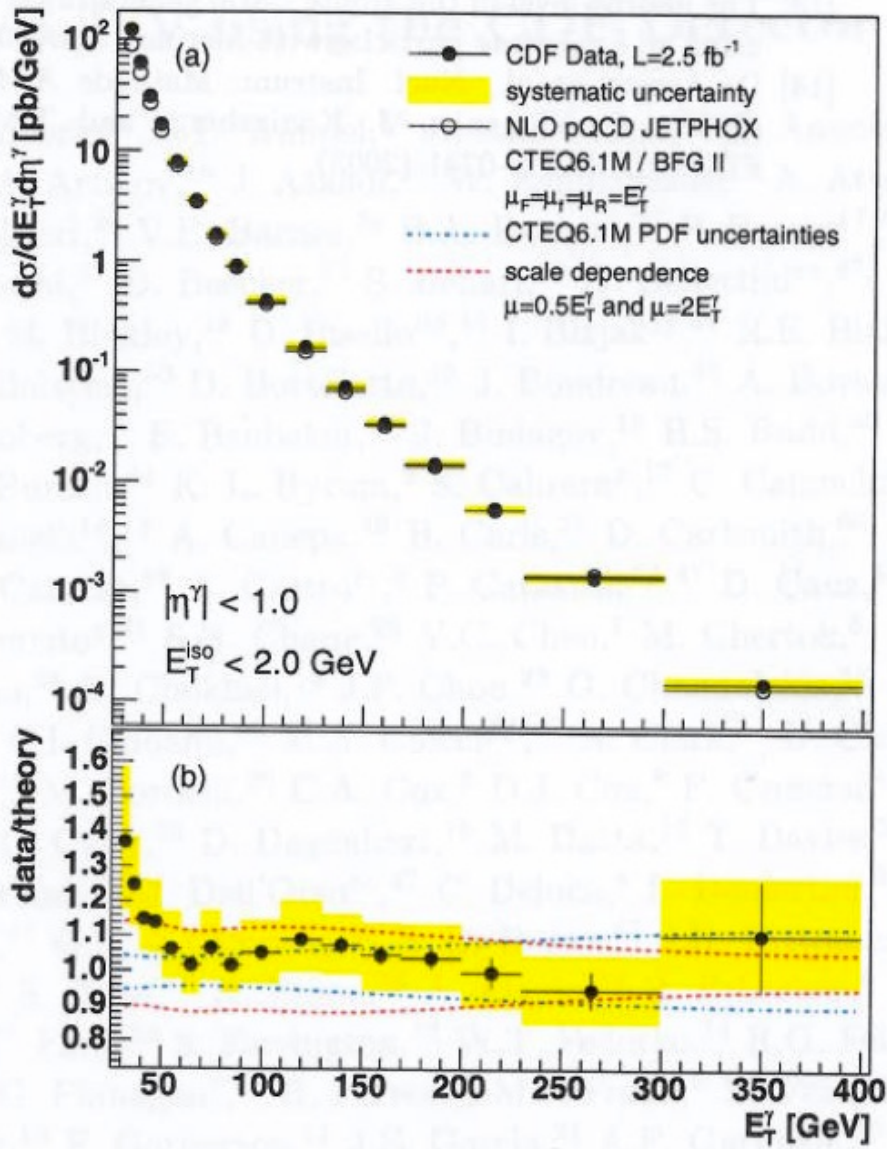
$$d(z) = \frac{\alpha_s}{2\pi} \frac{4}{3} (1 + z^2) \left(\frac{\ln(1 - z)}{1 - z} \right)_+ + \dots$$

Becher,Schwarz (SCET)

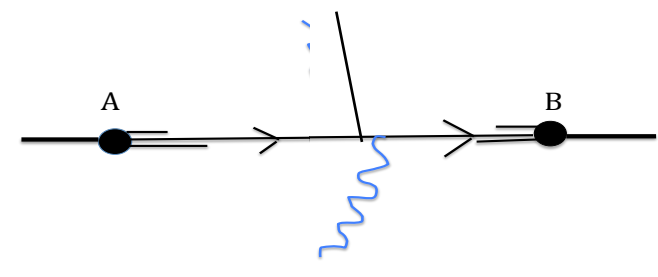
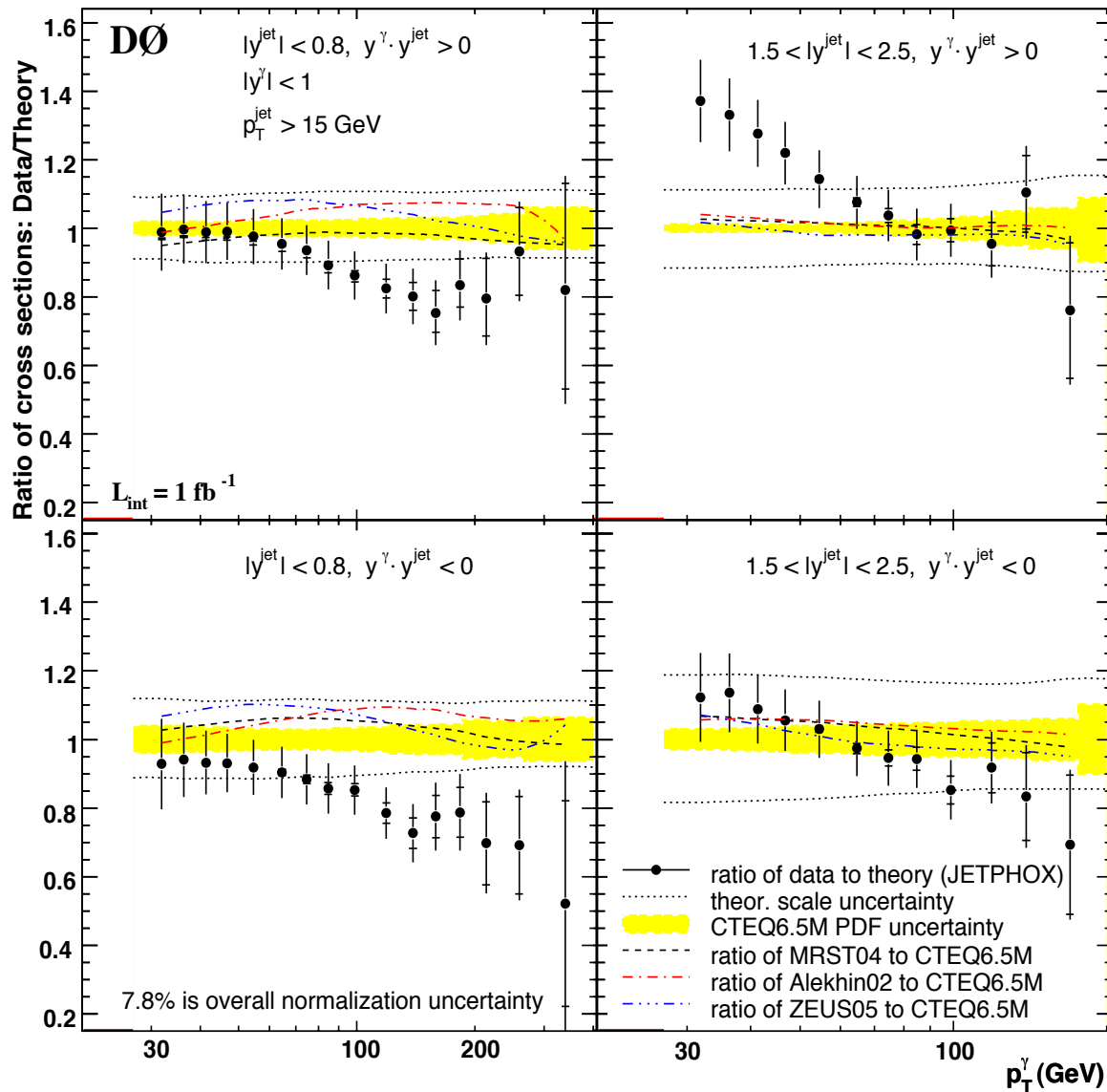
P. Aurenche et al. / Higher order QCD predictions







Photon-jet correlations



$$X_{\text{LL}} = \frac{p_T^{\gamma} (e^{\eta_{-\gamma}} + e^{\eta_{-\text{jet}}})}{\sqrt{s}}$$

$$X_{\text{obs}} = \frac{p_T^{\gamma} e^{\eta_{-\gamma}} + p_T^{\text{jet}} e^{\eta_{-\text{jet}}}}{\sqrt{s}}$$

LHC

ATLAS $15 < p_T^{\gamma} < 100 \text{ GeV}$ $R_c = .4$ $E_T^h < 4 \text{ GeV}$
 $45 < p_T^{\gamma} < 400 \text{ GeV}$

CMS $21 < p_T^{\gamma} < 300 \text{ GeV}$ $R_c = .4$ $E_T^h < 5 \text{ GeV}$
 $25 < p_T^{\gamma} < 400 \text{ GeV}$

fragmentation/total $\sim 20\text{-}25\%$ at low p_T
10% at large p_T (100 GeV)

JETPHOX $p_T/2 < \text{scales} < 2p_T$ $\sim 20\%$ (low p_T) 10% (large p_T)
PDF errors

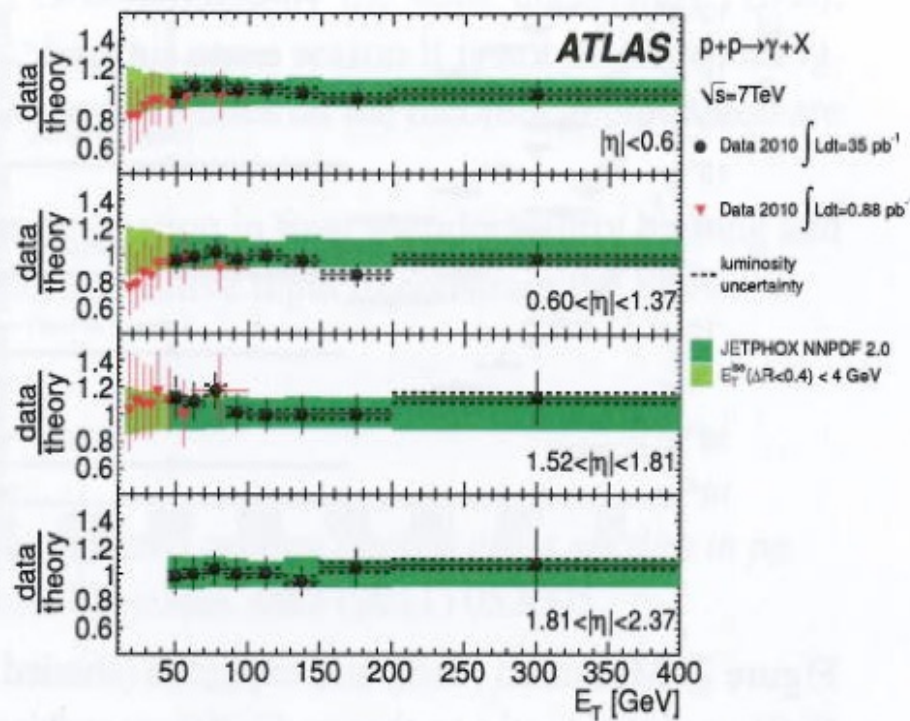
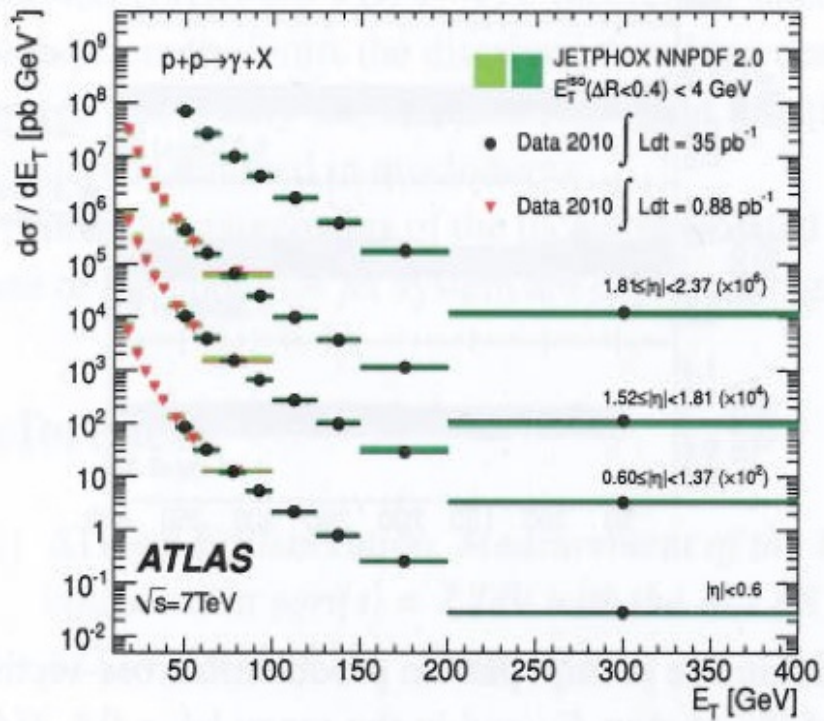
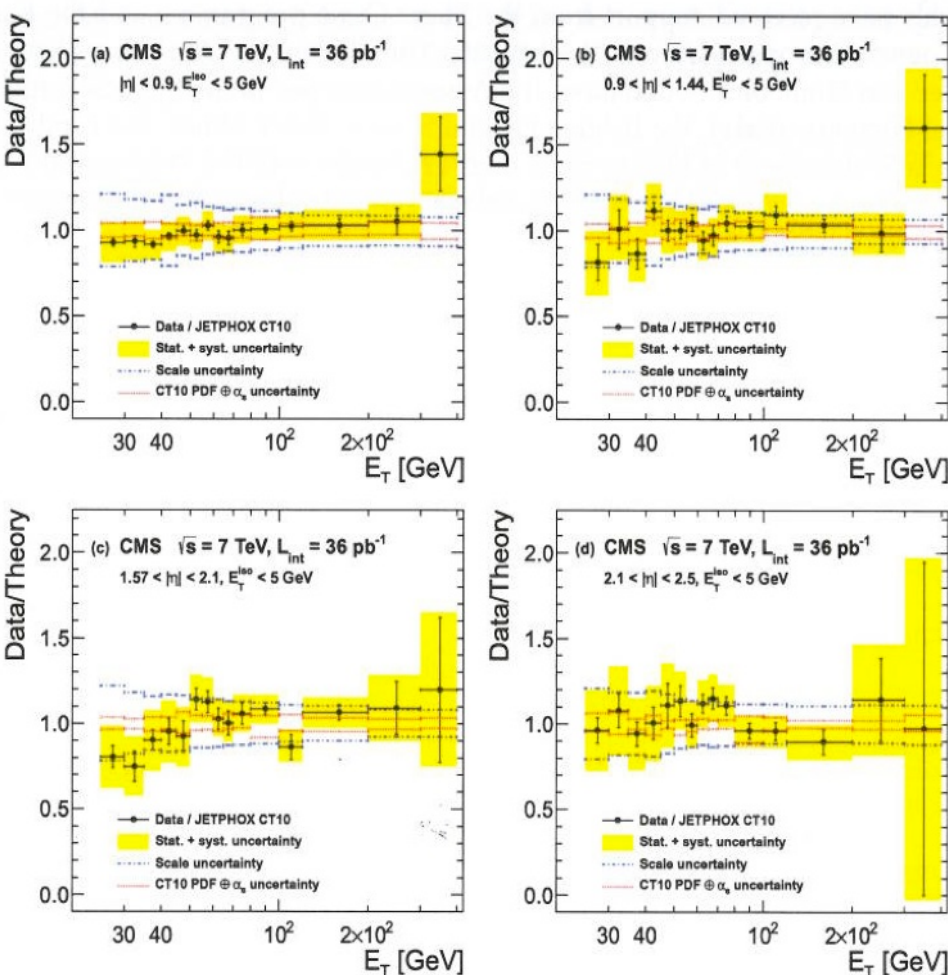
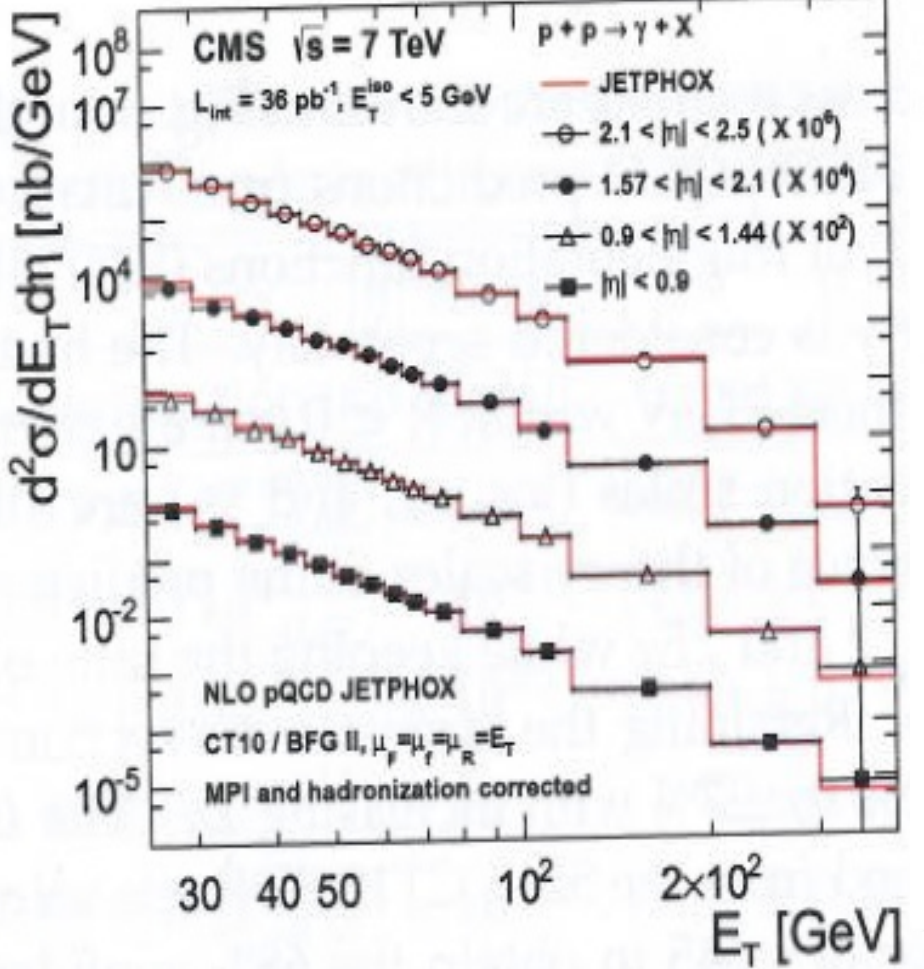


Figure 3: Measured (dots) and expected (shaded area) inclusive prompt photon production cross-sections (left), and their ratio to theory (right), as a function of the photon E_T and in the range $|\eta| < 0.6$, $0.6 \leq |\eta| < 1.37$, $1.52 \leq |\eta| < 1.81$ and $1.81 \leq |\eta| < 2.37$. The NNPDF 2.0 PDF is used in the JETPHOX theoretical computation (the full theoretical error is shown).



D'Enterria and Rojo

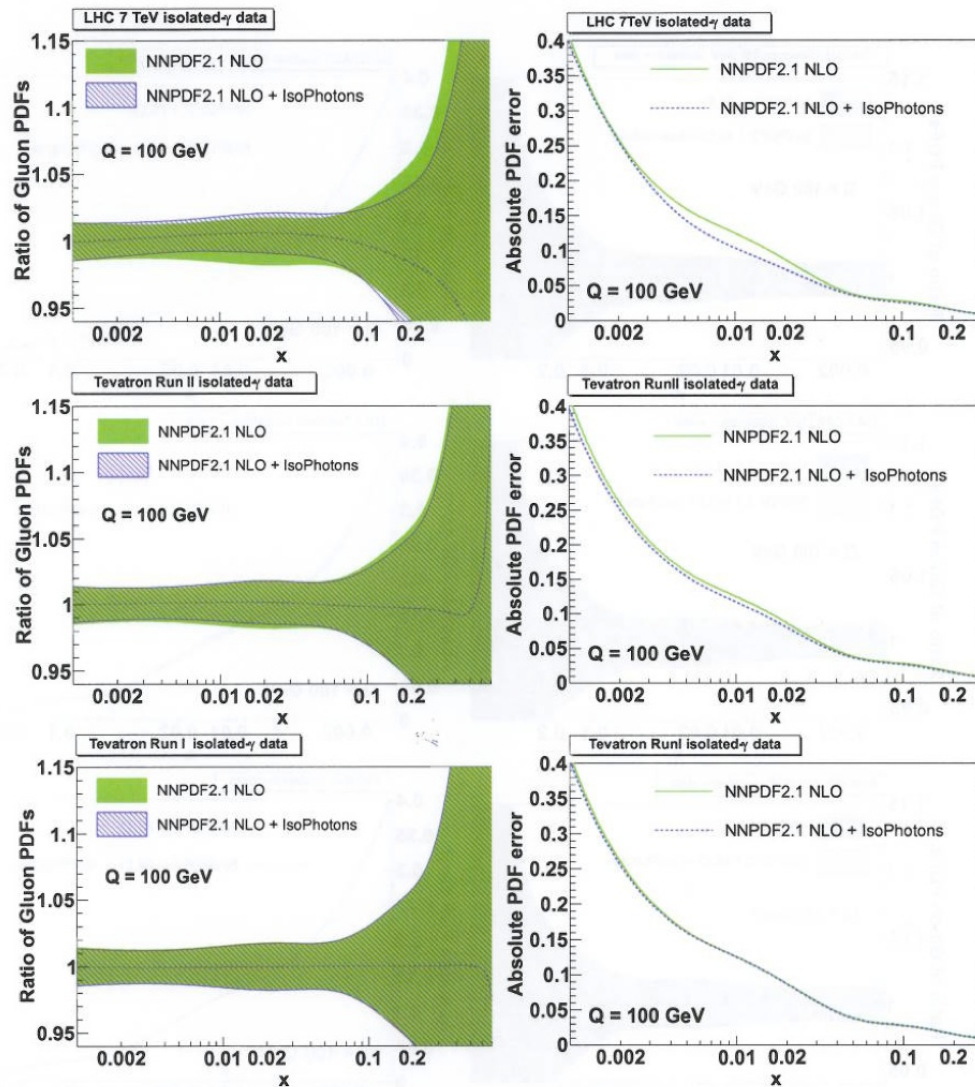


Figure 16: Comparison between the NNPDF2.1 NLO gluon before (green solid band) and after (dashed blue area) inclusion of the isolated- γ data from (top to bottom): LHC-7 TeV, Tevatron Run-II at 1.96 TeV, and Run-II at 1.8 TeV. The left plots show the ratio between the original and the new $g(x, Q^2)$ while the right panels indicates the reduction of absolute $g(x, Q^2)$ uncertainties thanks to the photon data. PDFs are valued at $Q = 100$ GeV, a typical LHC scale.

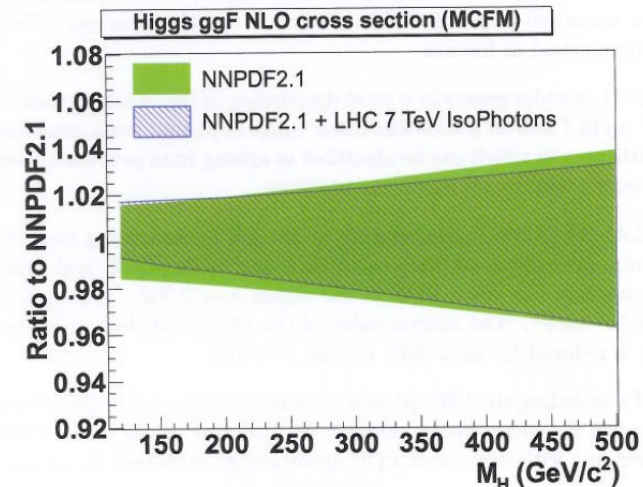
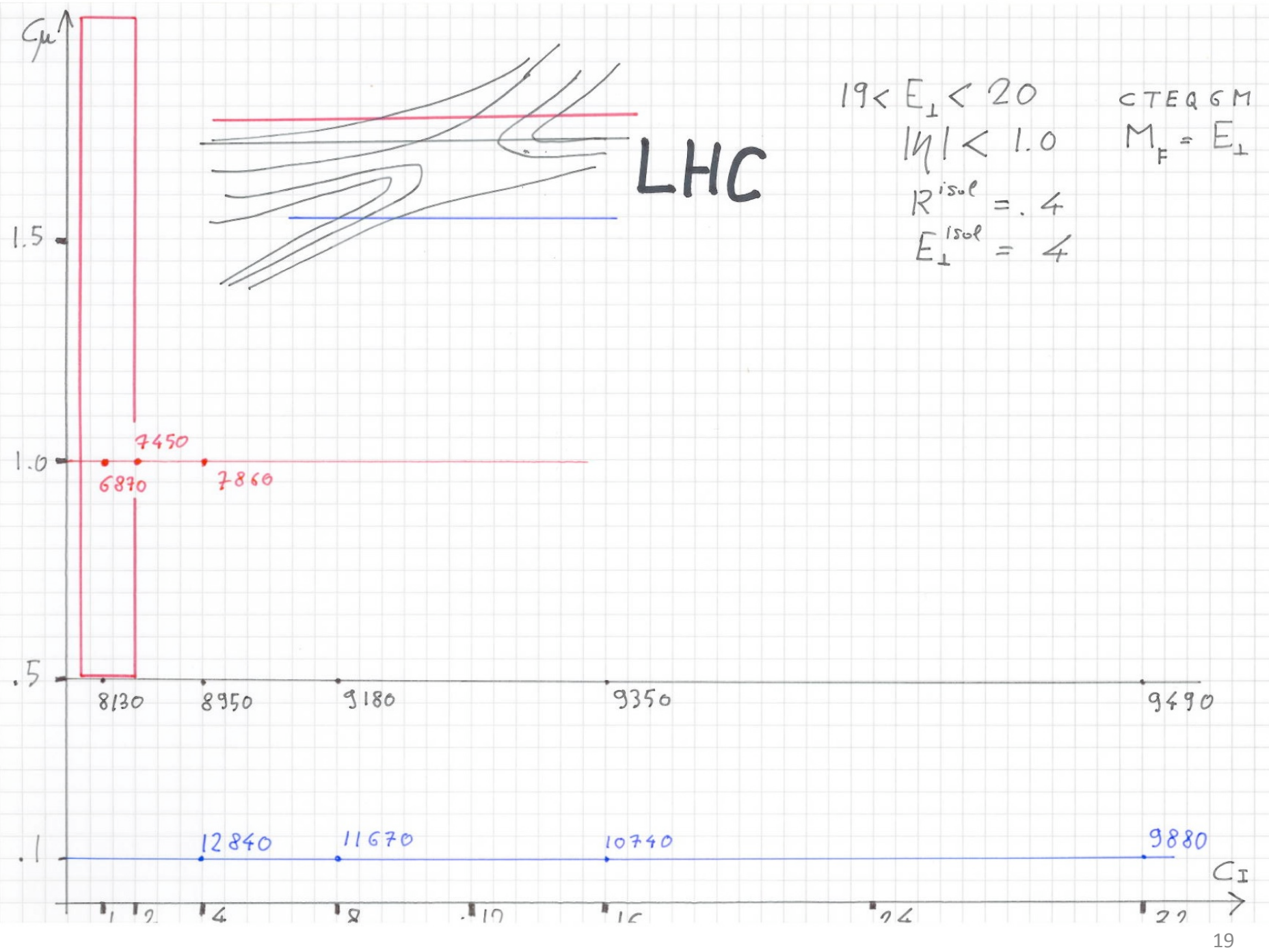


Figure 20: Ratio of Higgs production gluon-fusion cross sections with NNPDF2.1 NLO PDFs before and after including the LHC isolated-photon data.

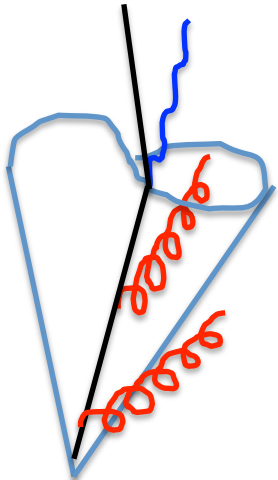
Fit including γ - jet correlations



Resummation of $\log(R_c^2)$

$$e_q^2 \frac{\alpha}{2\pi} P_{\gamma q}^{(0)}(z) \left\{ \left[\log \frac{R_c^2 p_\perp^\gamma}{M_F^2} + 2 \log(1-z) + \frac{z}{P_{\gamma q}^{(0)}} \right] \theta(z - z_c) + \log \frac{1}{R_c^2 z (1-z)} \right\} = e_q^2 \frac{\alpha}{2\pi} P_{\gamma q}^{(0)}(z) \log \frac{1}{R_c^2} \theta(z_c - z) + \dots$$

Catani et al.



$$D_q^\gamma(R_c p_\perp^\gamma, z) \quad \rightarrow \quad M_F = R_c p_\perp^\gamma$$

$$e^{\int_{(R_c p_\perp^\gamma)^2}^{(p_\perp^\gamma)^2} \frac{dk^2}{k^2} \frac{\alpha_s}{2\pi} p_{qq}^{(0)}} = 1 + \int \frac{dk^2}{k^2} \frac{\alpha_s}{2\pi} P_{qq}^{(0)}$$

$$D(R_c p_\perp^\gamma, p_\perp^\gamma, n) = \int_{(R_c p_\perp^\gamma)^2}^{(p_\perp^\gamma)^2} \frac{dk^2}{k^2} K e^{\int_{k^2}^{p_\perp^\gamma} \frac{dq^2}{q^2} \frac{\alpha_s}{2\pi} P_{qq}^{(0)}}$$

R	$\text{NLO}(p_\perp^\gamma/2)$	$\text{NLO}(Rp_\perp^\gamma)$	$\text{NLO}(Rp_\perp^\gamma)$ -resummed
.5	3.59	3.59	3.57
.3	3.86	3.85	3.81
.1	4.35	4.34	4.19
.06	4.56	4.55	4.24
.02	5.03	5.02	4.56
No isol ⁿ	4.29	4.72	4.72

Guillet
Pilon
MF

Table 3: Variation with R of the total cross sections at $\sqrt{s} = 7$ TeV (pb)

Monte Carlo approach

ALPGEN

Herwig

Pythia

Sherpa (Hoeche,Schuman,Siegert)

GR@PPA (Odaka,Kurihara)

Quark Reggeization (BFKL)

Saleev

k_T -factorization

small x_T limit

Baranov

Hautman

Jung

A.V.Lipatov

Pietrycki

Szcurek

Zotov

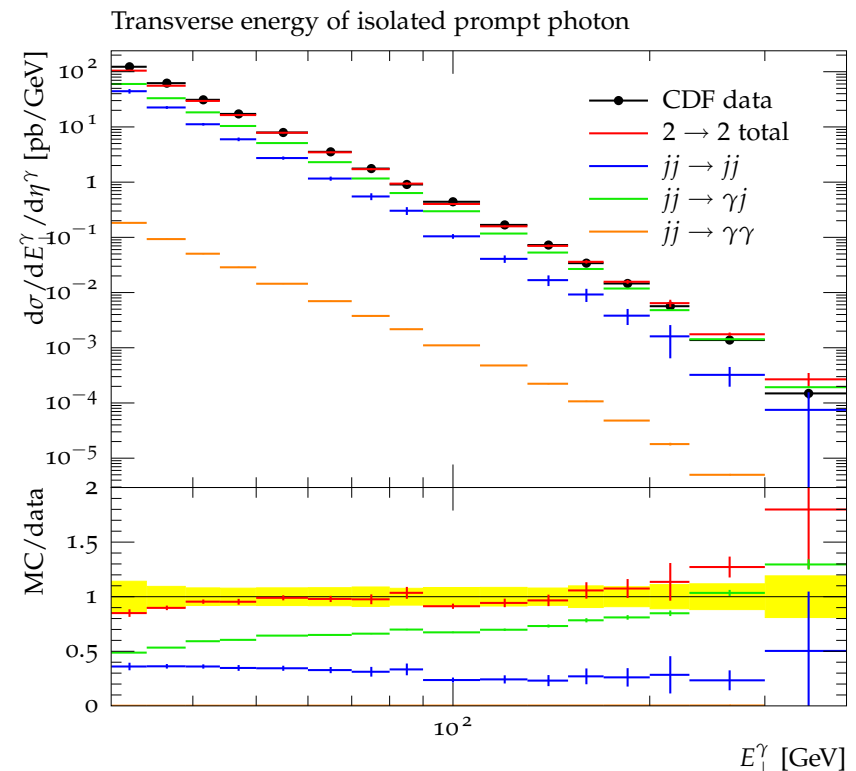
$$\sigma = \int dz d\vec{k}_\perp g(z, k_\perp) \hat{\sigma}(z, \vec{k}_\perp, \vec{p}_\perp^\gamma, S)$$

$$G(z, M^2) = \int_0^{M^2} d\vec{k}_\perp g(z, k_\perp)$$

Small- x resummation

(Diana,Rojo,Ball)

A few percents at $p_T < 10$ GeV



DIPHOTONS

ResBos (Balazs,Berger,Nadolsky,Yuan): Soft gluon resummation $\rightarrow d\sigma/dQ_T \xrightarrow{>} Q_T = p_{T1} + p_{T2} \xrightarrow{>} \gamma \gamma$

DIPHOX (Binoth,Guillet,Pilon,Werlen): Four different topologies at NLO
d-d, d-f, f-d, f-f Isolation (cone, Frixione)

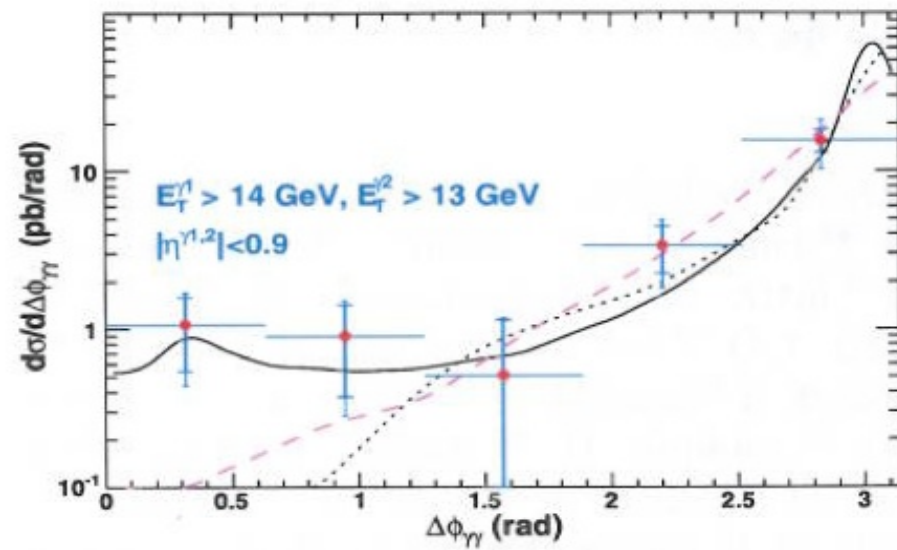
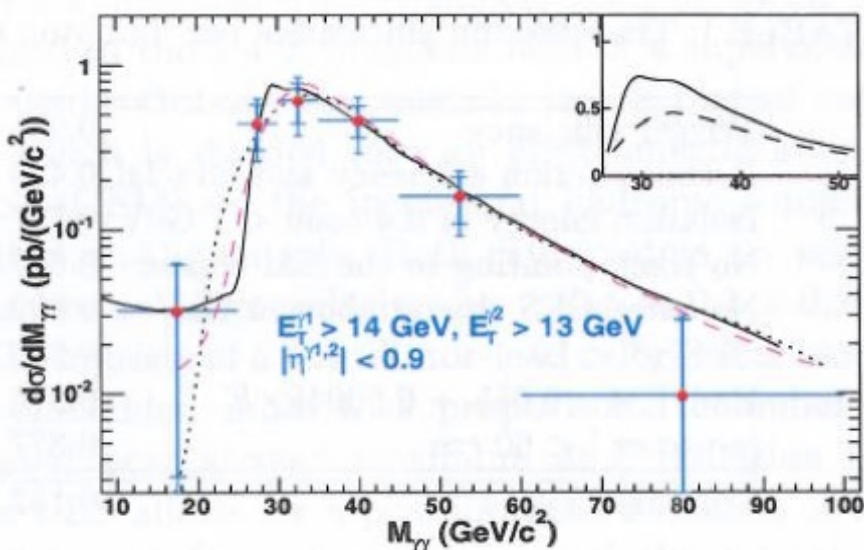
2gammaMC (Bern, Dixon and Schmidt) BOX at NLO

2 γ + jet @ NLO (Del Duca,Maltoni,Nagy,Trocsany)

MC@NLO (d'Errico and Richardson) (powheg)

MFCM (Campbel,Ellis and Williams) ~DIPHOX, with fragmentation at LO

2 γ NNLO (Catani,Cieri,de Florian,Ferrera and Grazzini)



CdF (2005)

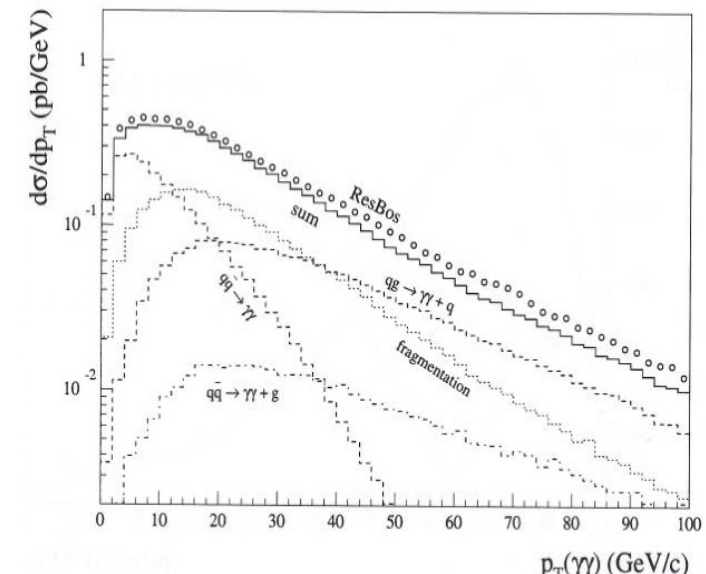
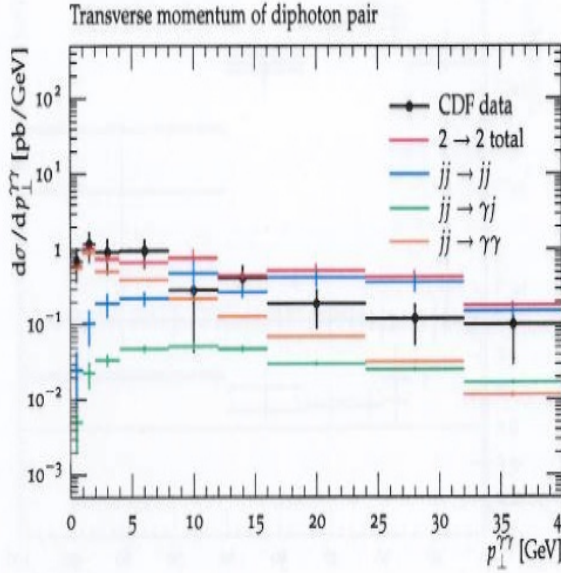
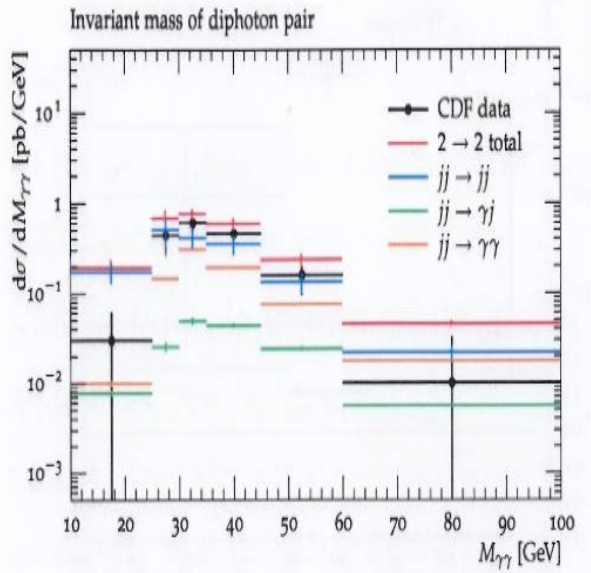
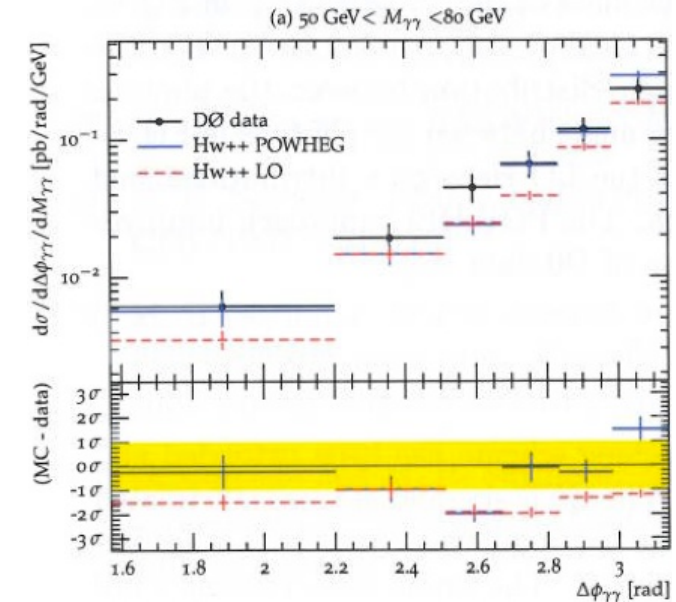
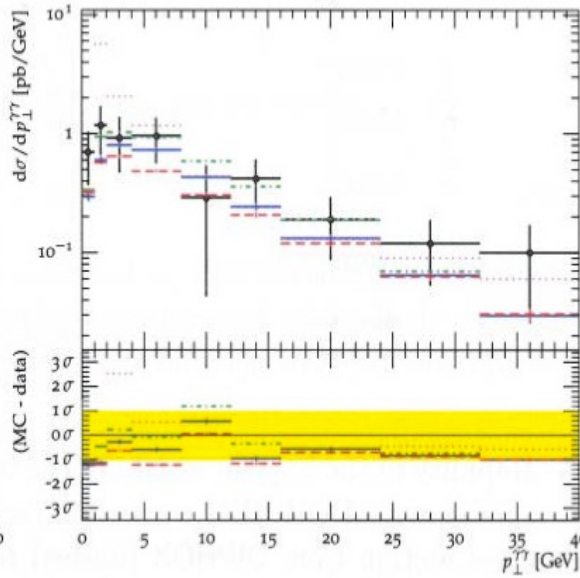
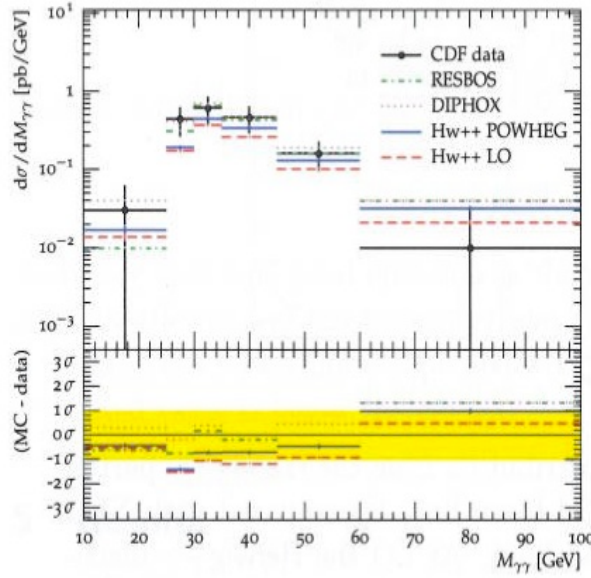


Figure 4: Properties of diphoton events measured by CDF [40]. Displayed are the sub-contributions from different leading-order matrix elements and their sum.

(A)Symmetric Pairs

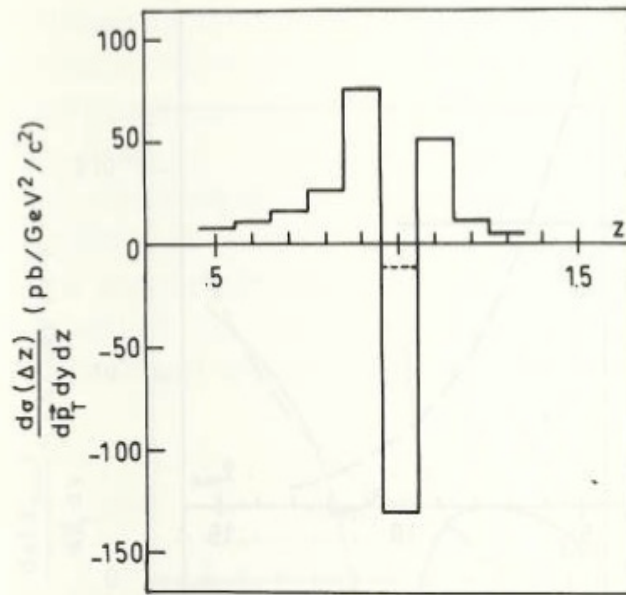


Fig. 9. Same as on Fig. 7, but for $p_T = 2 \text{ GeV}/c$

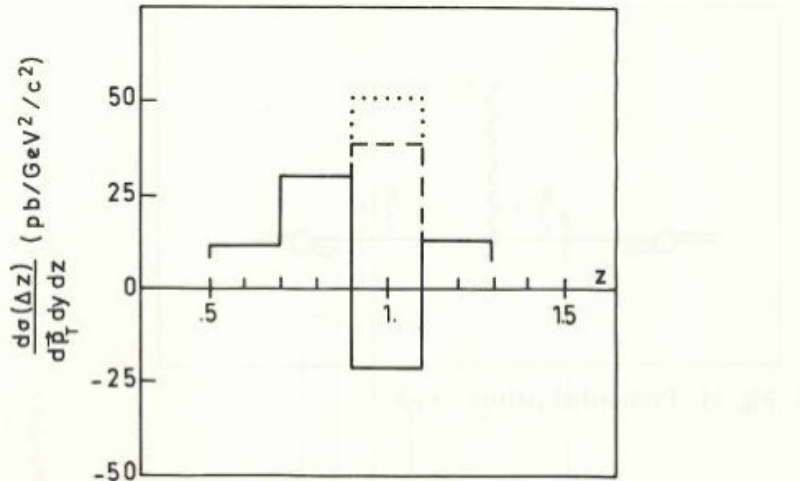
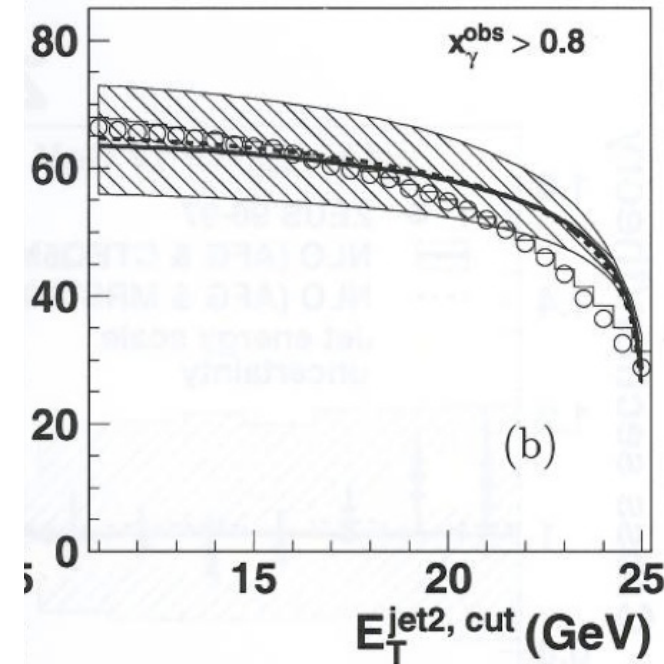
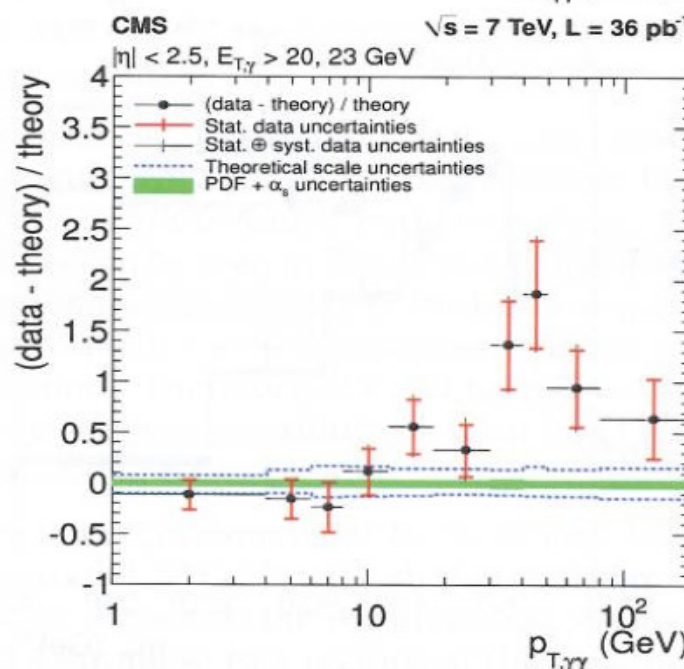
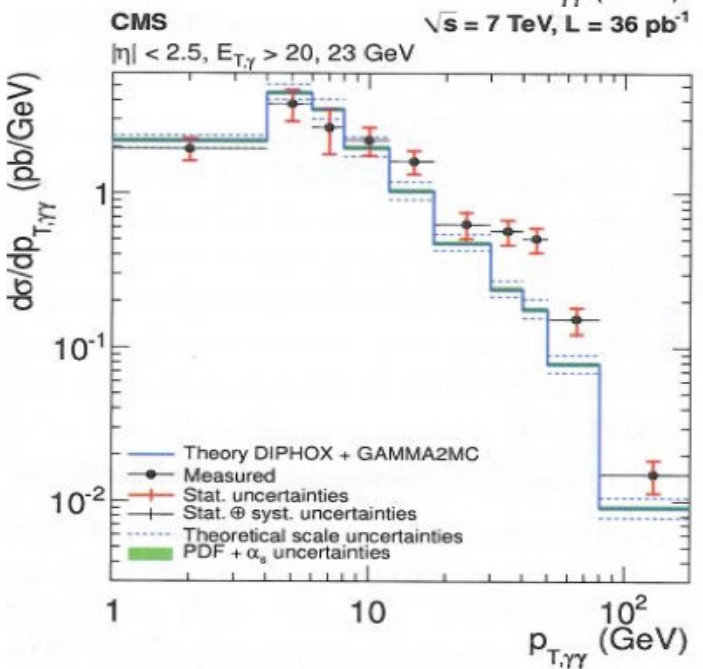
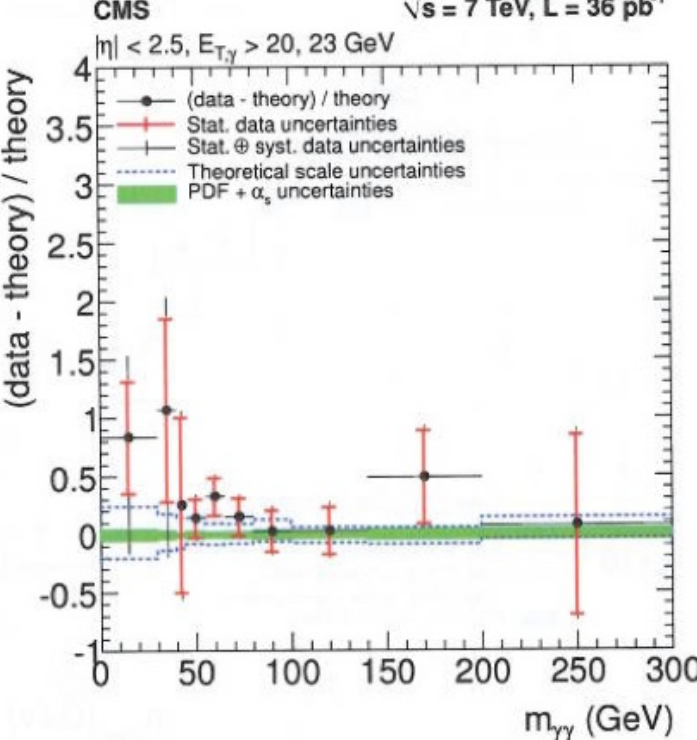
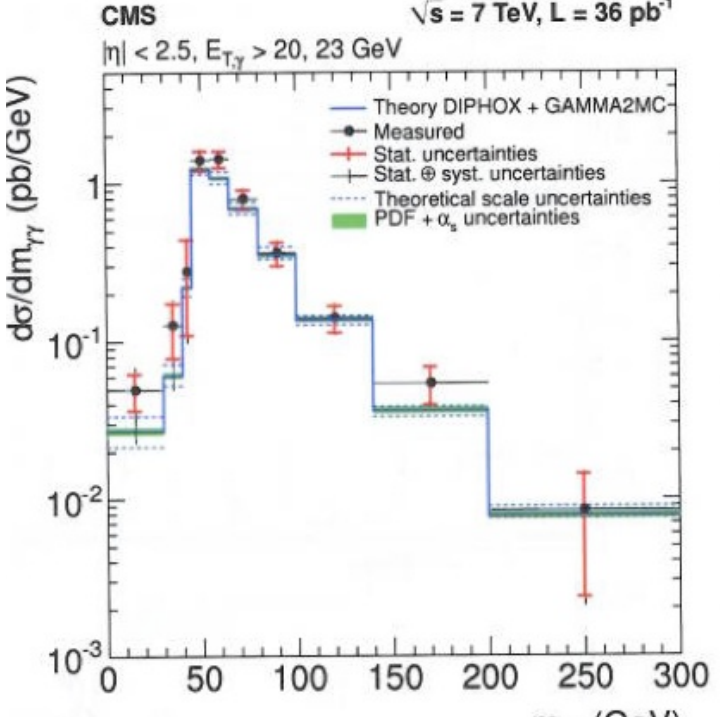


Fig. 10. Same as Fig. 9 but with a different binning $\Delta z = 0.2$. The dotted curve is the Born + Box + BLL contribution in the bin around $z = 1$

Aurenche et al. (1985)



- ZEUS 96-97
- HERWIG (normalised)
- ▨ NLO (GRV) \otimes HAD
- NLO (AFG) \otimes HAD



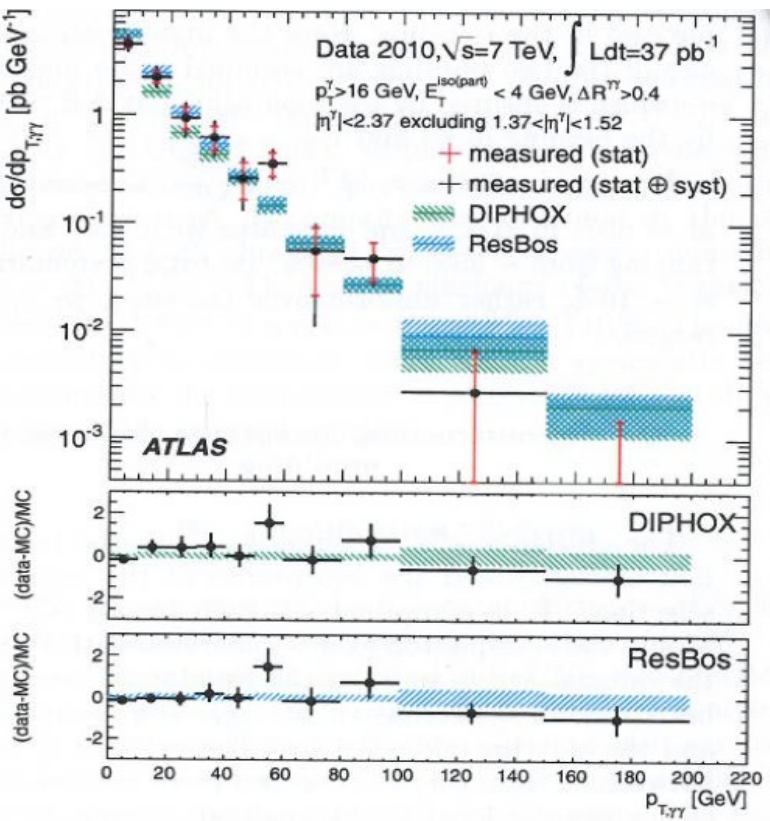


FIG. 8. Differential cross-section $d\sigma/dp_{T,\gamma\gamma}$ of di-photon production. The solid circles display the experimental values, the hatched bands display the NLO computations by DIPHOX and ResBos. The bottom panels show the relative difference between the measurements and the NLO predictions. The data point in the bin $150 < p_{T,\gamma\gamma} < 200$ GeV in the main panel lies below the frame.

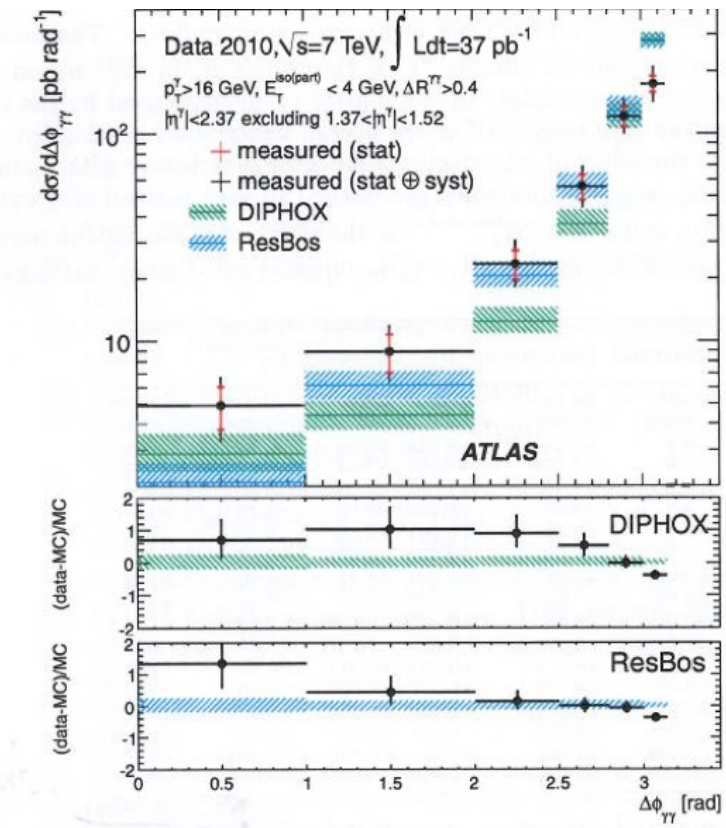
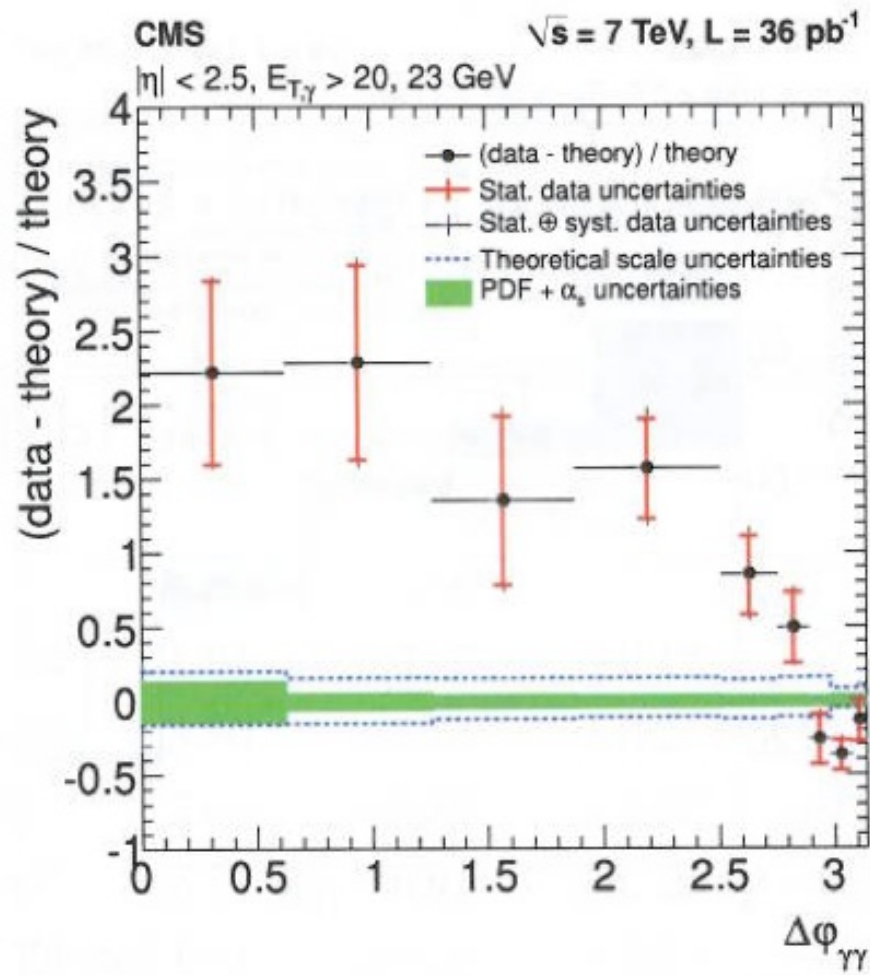
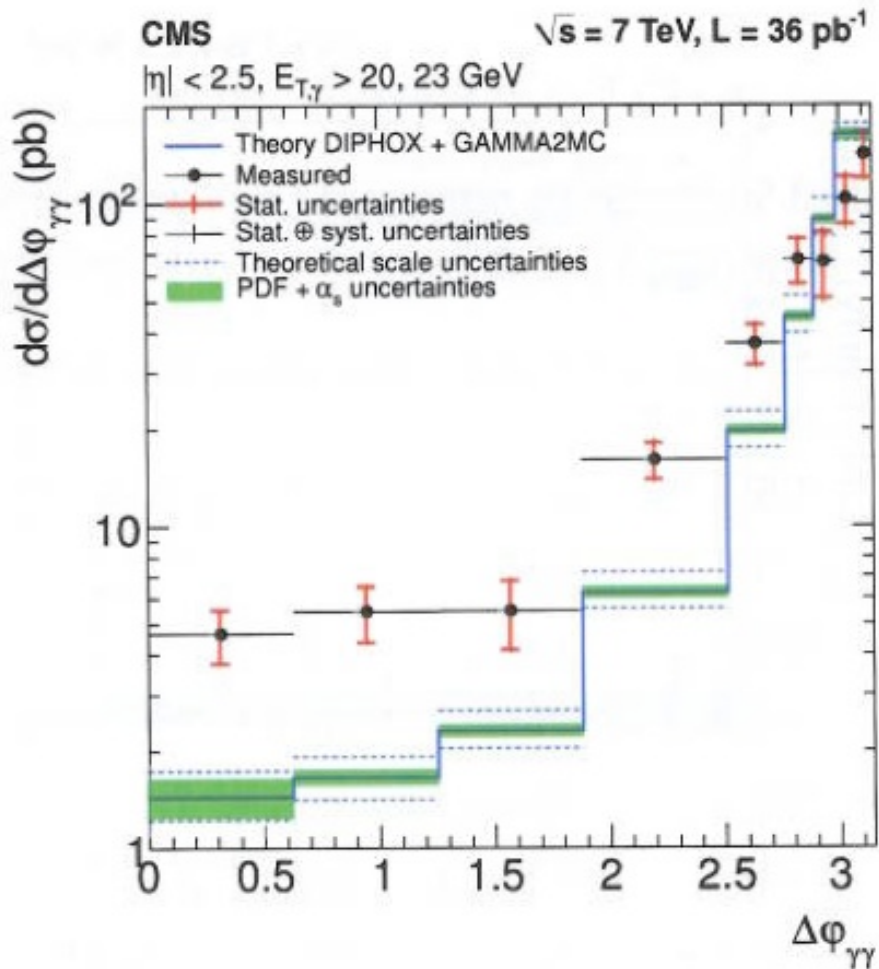


FIG. 9. Differential cross-section $d\sigma/d\Delta\phi_{\gamma\gamma}$ of di-photon production. The solid circles display the experimental values, the hatched bands display the NLO computations by DIPHOX and ResBos. The bottom panels show the relative difference between the measurements and the NLO predictions.



2gammaNNLO

$p_T^1 > 40 \text{ GeV}$
 $p_T^2 > 25 \text{ GeV}$
 $-2.5 < y < 2.5$
 $20 \text{ GeV} < M_{\gamma\gamma} < 250 \text{ GeV}$

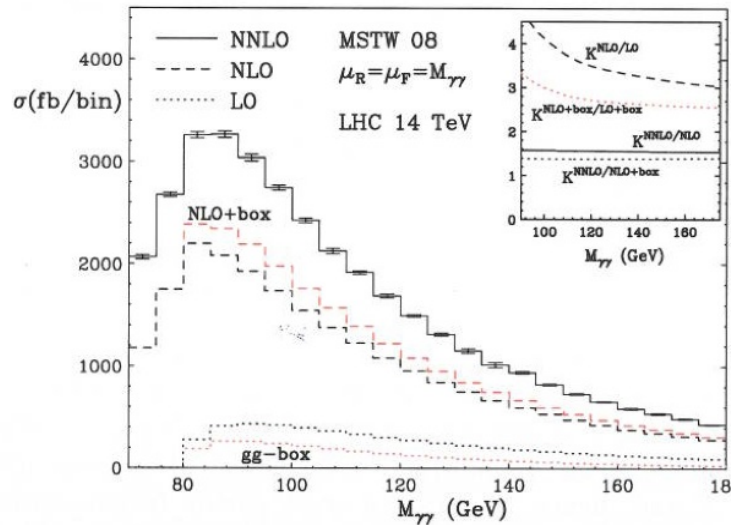


Figure 1: Invariant mass distribution of the photon pair at the LHC ($\sqrt{s} = 14 \text{ TeV}$): LO (dots), NLO (dashes) and NNLO (solid) results. We also present the results of the box and NLO+box contributions. The inset plot shows the corresponding K-factors.

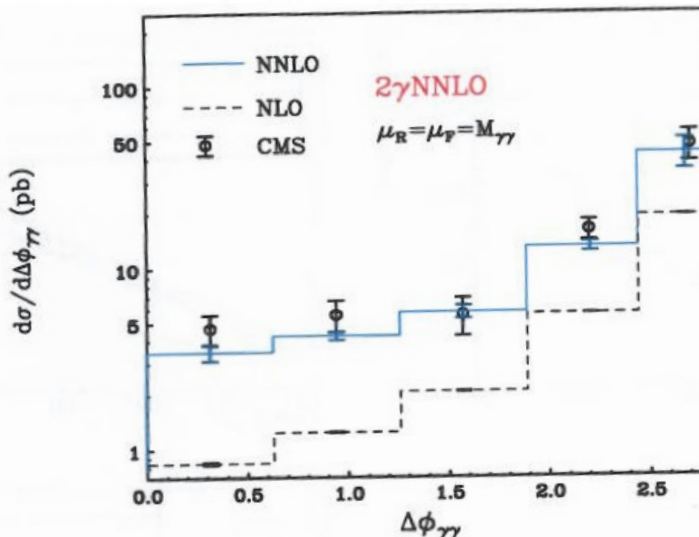
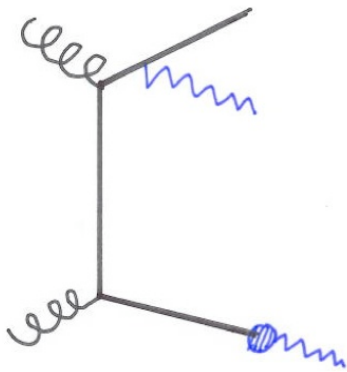
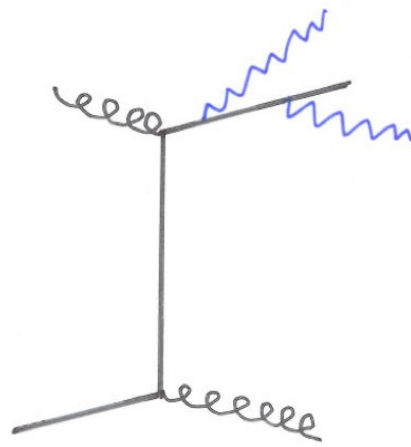
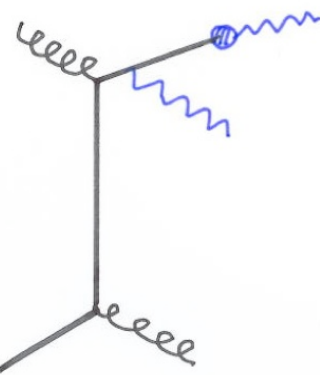
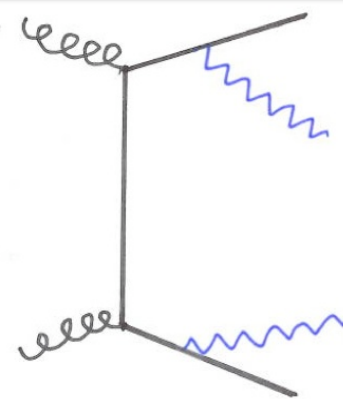


Fig. 77: Differential diphoton cross section as a function of $\Delta\phi_{\gamma\gamma}$ at NNLO (blue) and at NLO (dotted black) calculated with a preliminary result from the 2GAMMANNLO program, superimposed on results from CMS data (points) from 2010 [311].

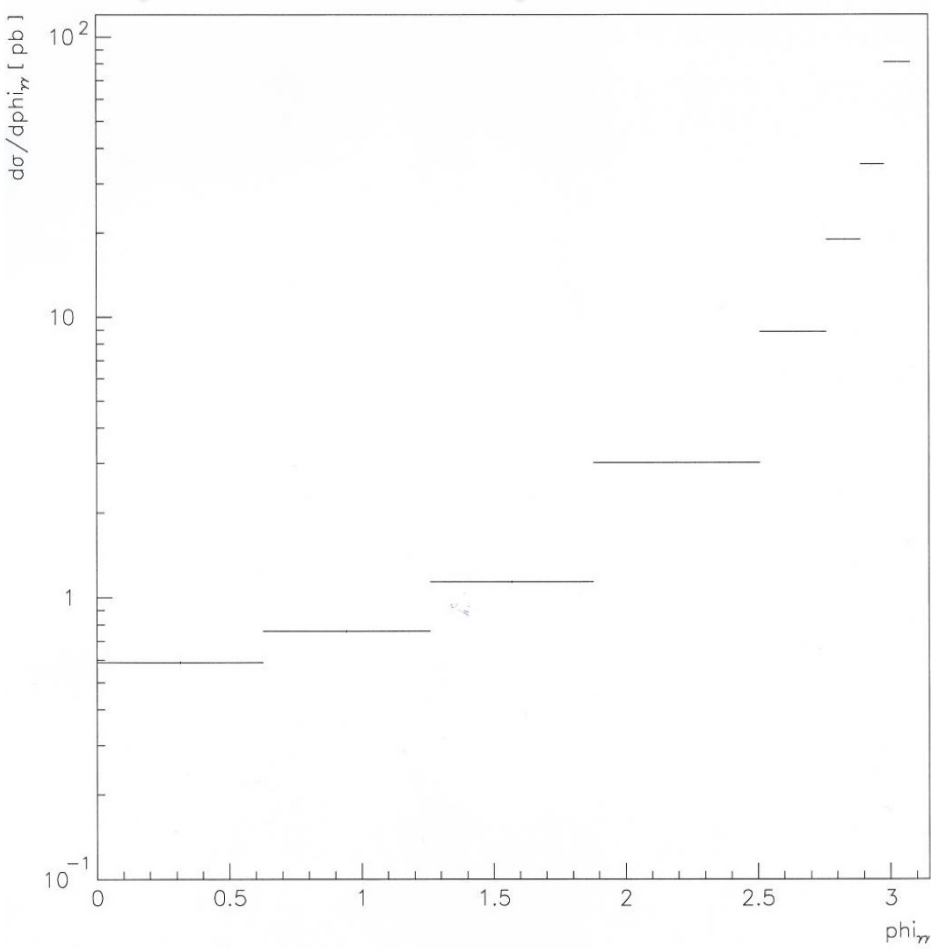
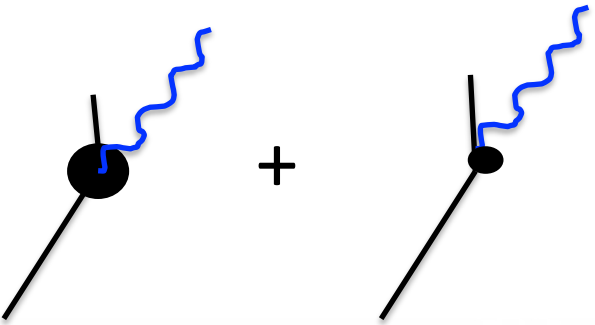
NLO



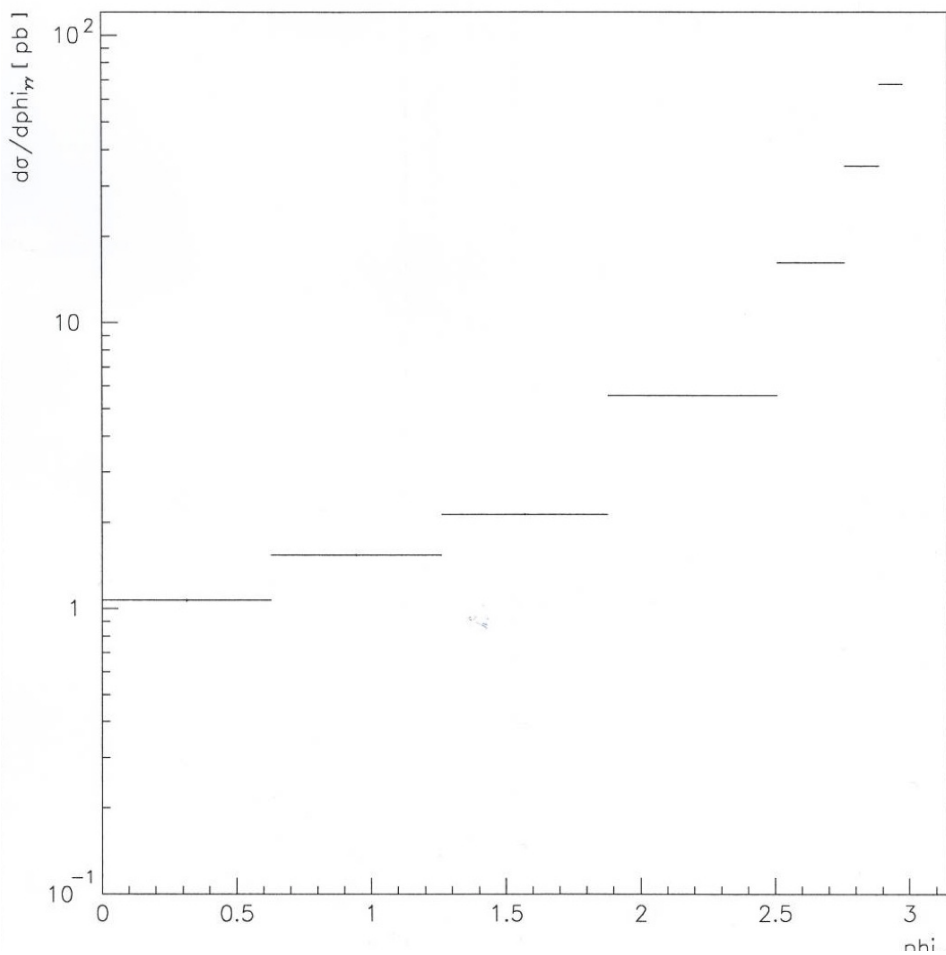
NNLO



Enhanced direct-fragmentation component



Very preliminary (guillet,pilon,mf)



CONCLUSION

